

# Identification of First-in-Class Inhibitors of Kallikrein-Related Peptidase 6 That Promote Oligodendrocyte Differentiation

Sabrina Aït Amiri, Cyrille Deboux, Feryel Soualmia, Nancy Chaaya, Maxime Louet, Eric Duplus, Sandrine Betuing, Brahim Nait Oumesmar,\* Nicolas Masurier,\* and Chahrazade El Amri\*

**Cite This:** *J. Med. Chem.* 2021, 64, 5667–5688

**Read Online**

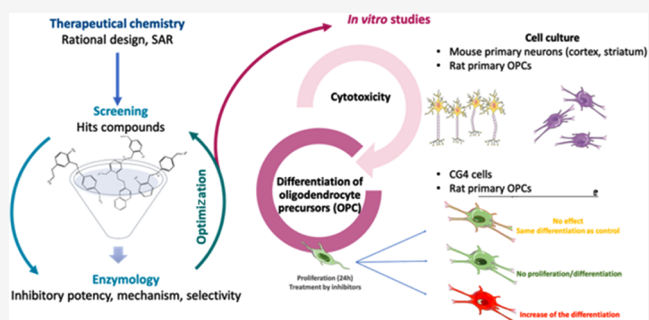
ACCESS |

Metrics & More

Article Recommendations

Supporting Information

**ABSTRACT:** Multiple sclerosis (MS) is an autoimmune demyelinating disease of the central nervous system (CNS) that causes severe motor, sensory, and cognitive impairments. Kallikrein-related peptidase (KLK)6 is the most abundant serine protease secreted in the CNS, mainly by oligodendrocytes, the myelin-producing cells of the CNS, and KLK6 is assumed to be a robust biomarker of MS, since it is highly increased in the cerebrospinal fluid (CSF) of MS patients. Here, we report the design and biological evaluation of KLK6's low-molecular-weight inhibitors, *para*-aminobenzyl derivatives. Interestingly, selected hit compounds were selective of the KLK6 proteolytic network encompassing KLK1 and plasmin that also participate in the development of MS pathophysiology. Moreover, hits were found nontoxic on primary cultures of murine neurons and oligodendrocyte precursor cells (OPCs). Among them, two compounds (32 and 42) were shown to promote the differentiation of OPCs into mature oligodendrocytes *in vitro* constituting thus emerging leads for the development of regenerative therapies.



## INTRODUCTION

Multiple sclerosis (MS) is a chronic inflammatory demyelinating disease of the central nervous system (CNS). MS affects more than two million people worldwide.<sup>1</sup> In young adults, MS is the most common neurological disorder and the leading cause of severe nontraumatic disability. The main target of MS is the myelin sheath surrounding CNS axons in the brain, spinal cord, and optic nerve.<sup>1</sup> The myelin sheath is synthesized by oligodendrocytes (OLs) that play a crucial role in the maintenance and functioning of neuronal networks. MS is associated with an inflammatory reaction of the CNS that results in degradation of the myelin sheath, therefore leading to diffuse demyelinating lesions. The consequences of this demyelination are multiple: nerve conduction is impaired and neurodegeneration occurs with disease progression.<sup>2</sup> Moreover, myelin debris exacerbates the activation of immune pathways triggering demyelination.<sup>3</sup> Clinically, these disturbances result in severe motor, sensory, and cognitive deficits. The lack of a regenerative therapy that prevents disease progression represents the greatest unmet medical in MS. Disease-modifying drugs in the market are mainly targeting the inflammatory components of the pathology, but have little impact on oligodendrocyte regeneration and remyelination.<sup>4–6</sup> The identification of new therapeutic compounds for MS-enhancing myelin repair is thus a critical public health issue.<sup>7,8</sup> A special effort may be put on the search for pharmacological compounds, capable of simultaneously modulating neuro-

inflammation and promoting myelin regeneration for more complete health care of MS patients. There is thus an urgent need to identify and validate novel targets to reach this issue.

In adults, under normal physiological conditions, kallikrein-related peptidase 6 (KLK6) is strongly expressed by oligodendrocytes and can be detected in neurons, whereas it is very weakly expressed in astrocytes and resting microglia.<sup>9</sup> However, in response to a CNS lesion such as glutamate-induced excitotoxicity, inflammation, or traumatic injury, the level of KLK6 expression rises in oligodendrocytes and neurons, and its expression is induced in reactive astrocytes and microglia.<sup>10</sup> Among the 15 tissue kallikreins, KLK6 is the most abundant in the CNS, and is arguably the most abundant serine proteases produced in the CNS.<sup>11</sup>

KLK6 has a versatile action within the CNS.<sup>9</sup> Interestingly, KLK6 cleaves myelin proteins, such as the myelin basic protein (MBP). KLK6 is a major protease of the process of demyelination/remyelination of axons.<sup>9,10,12</sup> In addition to cleaving myelin proteins, KLK6 can also degrade blood–brain barrier components such as laminin, fibronectin, and collagen,

**Received:** December 16, 2020

**Published:** May 5, 2021



Scheme 1. Putative KLK6's Pathological Proteolytic Network

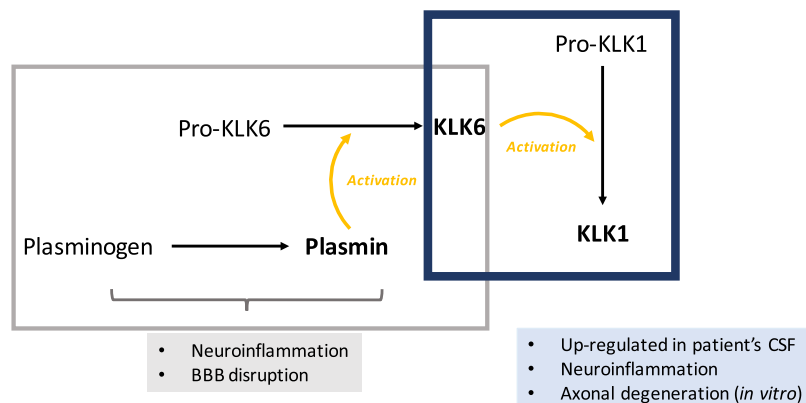
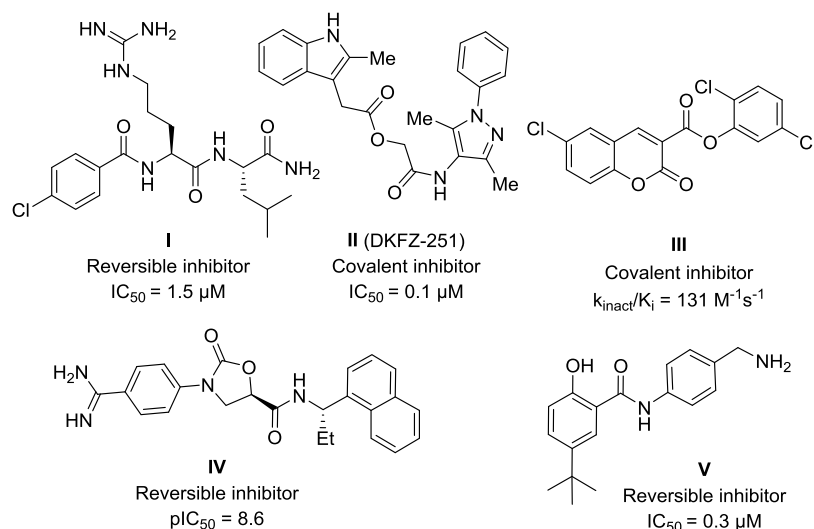


Chart 1. Main KLK6 Inhibitors Reported in the Literature



and therefore induce inflammation *via* protease-activated receptors (PAR) activation and underlying intracellular  $Ca^{2+}$  mobilization. It should also be noted that the use of recombinant KLK6 *in vitro* contributes to neuronal lesions and oligodendroglipathies.<sup>13</sup> Some proteases have also been suggested for the activation of KLK6 *in vivo*, including plasmin, a serine protease involved in fibrinolysis. Finally, KLK6 is involved in oligodendrocyte differentiation and myelination processes. Different studies support that KLK6 is involved in the pathophysiology of MS.<sup>12–17</sup> First, patients with MS have abnormally high KLK6 levels in serum, cerebrospinal fluid (CSF), and demyelinating lesions, which demonstrate the implication of this protease at different levels of the pathology.<sup>18</sup> Second, KLK6 induces demyelination, through both excessive cleavage of myelin proteins and deleterious effects on oligodendrocyte-process outgrowth and differentiation, thus leading to a drastic reduction in the number of myelinating oligodendrocytes.<sup>19</sup> Third, KLK6 participates in the neuroinflammatory process through the overactivation of PAR receptors and also by increasing the expression of proinflammatory cytokines. Therefore, KLK6 participates in the establishment of a toxic environment that leads to demyelination and neurodegeneration, the main causes of disability progression in MS patients.<sup>19</sup> KLK6 and KLK1 may also serve as serological markers of MS and may contribute directly to neurodegeneration. Furthermore, the immunization

of mice with recombinant KLK6 antibodies significantly delayed onset and severity of clinical deficits in an experimental autoimmune encephalomyelitis (EAE) mouse model of MS.<sup>12,20</sup> It is also well established that the potential significance of proteolytic activity in MS not only relates to their use as potential biomarkers but also as prospective therapeutic targets. The range of potential involvement of proteolytic activity in MS pathogenesis extends from parenchymal degenerative events, including myelin destruction and axon injury, to release of antigenic self-epitopes, immune cell activation, and permeabilization of the blood–brain barrier. Scarisbrick and co-workers have proposed the term of MS degradome to encompass the set of proteases, substrates, and endogenous protease inhibitors involved in the development and progression of MS.<sup>19</sup>

Scheme 1 summarizes the central role of KLK6 and its crosstalk with thrombolytic proteolytic pathways, thus illustrating the early concept of MS degradome.<sup>21</sup> Particularly, it has been recently shown that plasminogen and plasmin-mediated fibrinolysis are key modifiers of the onset of neuroinflammatory demyelination.<sup>22,23</sup> KLK1 was early shown to be a potential serological marker of progressive MS and contribute directly to the development of neurological disability by promoting axonal injury and neuron apoptosis.<sup>19</sup>

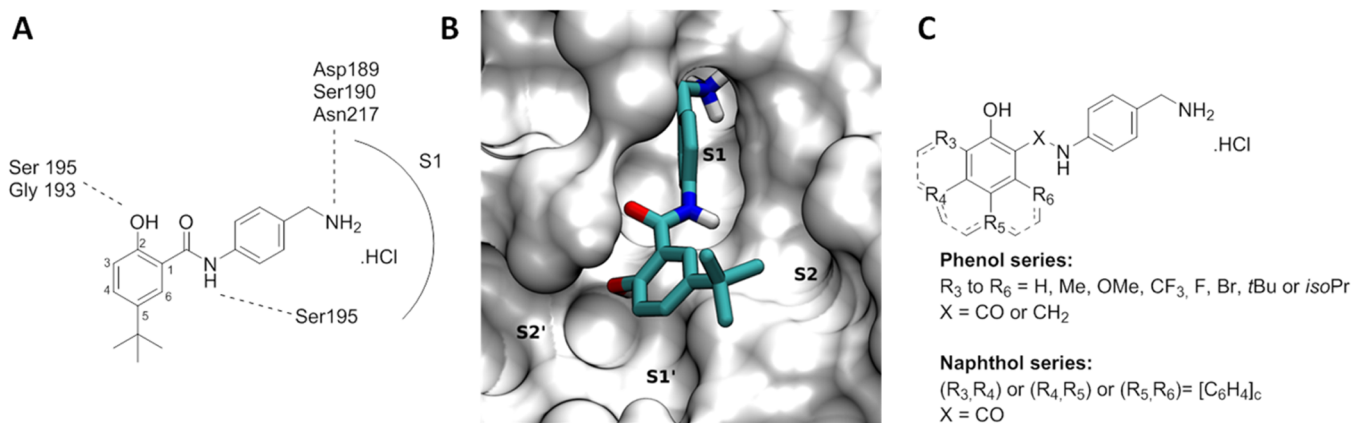
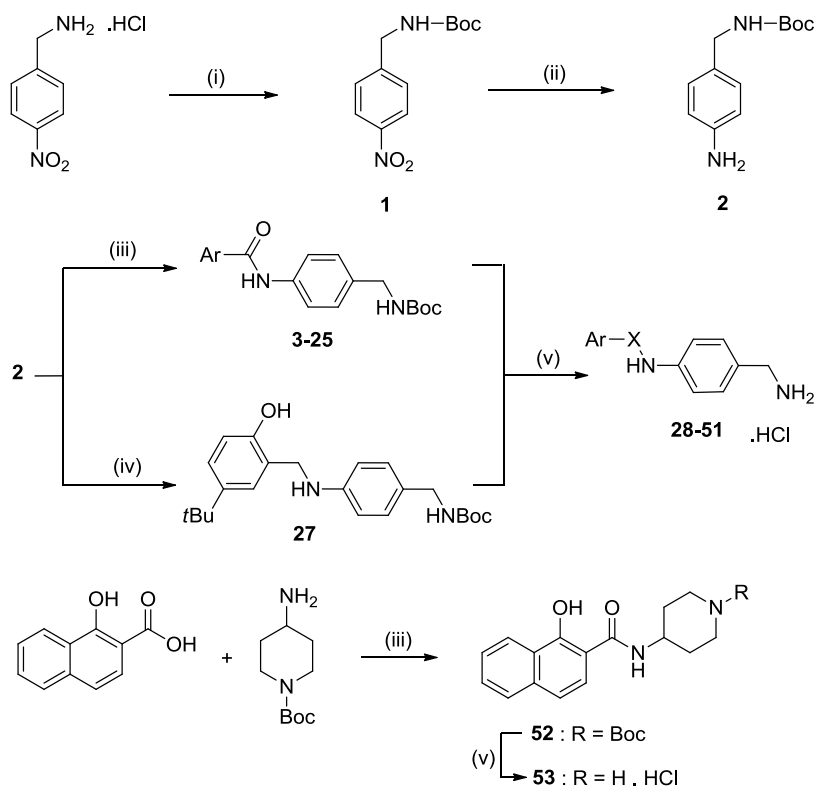


**Figure 1.** Rational design of *para*-amidobenzyl derivatives. (A) Key interactions of compound **V** in the active site of KLK6 (H bonds are shown as dashed lines); (B) positioning of compound **V** in the S1 and S1' pockets of KLK6; and (C) structures of studied compounds.

### Scheme 2. Synthesis of Compounds 1–53<sup>a</sup>



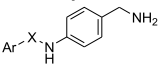
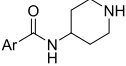
<sup>a</sup>Reagents and conditions: (i) Boc<sub>2</sub>O, triethylamine (TEA), dichloromethane (DCM), room temperature (RT), 2 h, 80%; (ii) H<sub>2</sub>, 10% Pd/C, AcOEt, RT, 4 h, qt; (iii) ArCO<sub>2</sub>H, *N*-(3-dimethylaminopropyl)-*N*'-ethylcarbodiimide hydrochloride (EDCI), tetrahydrofuran (THF), reflux, 12 h, 12–82%; (iv) (1) Compound **26**, EtOH, reflux, 6 h; (2) NaBH<sub>4</sub>, RT, 1.5 h, 64% and (v) 6 N HCl gas in 1,4-dioxane, RT, 1.5 h, 44–99%.

In this context, the development of innovative inhibitors of KLK6 activity and its associated proteolytic network appears as a new therapeutic avenue.

The aim of this study is thus to identify potent KLK6 inhibitors encompassing the following properties: (i) reversibility, indeed noncovalent inhibitors, which are devoid of a reactive group, do not have the drawbacks generally associated with the presence of a warhead, such as lack of specificity, instability, and excessive reactivity. Considering the physiological implication of KLK6 in the CNS homeostasis reversible inhibition would be safer, and (ii) able to inhibit other proteases involved in the KLK6 proteolysis network, *i.e.*, KLK1 and plasmin. Herein, we identified and optimized original

organic inhibitors for KLK6 and its proteolytic network. The designed low-molecular-weight inhibitors are potent and reversible toward KLK6, and their inhibitory potency was also evaluated on a large panel of proteases. We also provided a detailed structure–activity relationship (SAR) and dissected out the chemical basis for optimal inhibition. Hit compounds were found devoid of cytotoxic effects toward both primary cultures of mouse neurons and oligodendrocyte precursor cells (OPCs) and displayed favorable druglike characteristics. Interestingly, some hit compounds promoted OPC differentiation *in vitro*. These selected compounds constitute promising leads for the development of innovative myelination therapy.

Table 1. Efficacy of *para*-Aminobenzyl Compounds toward KLK6<sup>a</sup>

Compound 	Ar	X	% Inhibition at 10 $\mu$ M or IC <sub>50</sub> ( $\mu$ M)
28	5- <i>tert</i> -butyl-2-hydroxyphenyl	CO	9.06 $\pm$ 0.65
29	5- <i>tert</i> -butyl-2-hydroxyphenyl	CH <sub>2</sub>	NI
30	2-hydroxyphenyl	CO	14.83 %
31	3-methyl-2-hydroxyphenyl	CO	20%
32	4-methyl-2-hydroxyphenyl	CO	2.37 $\pm$ 0.12
33	5-methyl-2-hydroxyphenyl	CO	26.47 %
34	6-methyl-2-hydroxyphenyl	CO	7.27 %
35	5-bromo-2-hydroxyphenyl	CO	29.98 %
36	5-methoxy-2-hydroxyphenyl	CO	21.83 %
37	4-isopropyl-2-hydroxyphenyl	CO	3.63 $\pm$ 0.1
38	4-trifluoromethyl-2-hydroxyphenyl	CO	47 %
39	4-fluoro-2-hydroxyphenyl	CO	NI
40	1-hydroxy-2-naphthyl	CO	6.90 $\pm$ 0.24
41	2-hydroxy-1-naphthyl	CO	NI
42	3-hydroxy-2-naphthyl	CO	1.57 $\pm$ 0.03
43	2-naphthyl	CO	19.81 %
44	1-indolyl	CO	NI
45	4-oxo-3-quinolyl	CO	NI
46	2-pyridin-3-ol	CO	8.86%
47	6-methoxy-1-hydroxy-2-naphthyl	CO	7.18 $\pm$ 0.33
Compound 	Ar		% Inhibition at 10 $\mu$ M
53	1-hydroxy-2-naphthyl		NI

<sup>a</sup>For each compound, the inhibitory effect was quantified either by the percentage inhibition of KLK6 at 10  $\mu$ M or by the IC<sub>50</sub> for compound hits. To determine the IC<sub>50</sub>, compounds at different concentrations (concentration ranges adjusted depending on the inhibitory potency) are preincubated for 15 min at 37 °C with KLK6 (2 nM). The enzymatic reaction is triggered by the addition of the Boc-QAR-AMC substrate (100  $\mu$ M) in 50 mM Tris buffer, 1 M citrate 0.05% Brij-35; pH 7.4 at 37 °C. NA: not applicable. NI: noninhibitor. The data result from at least three independent experiments in duplicate. The IC<sub>50</sub> values were calculated by fitting the experimental data to eq 2a or eq 2b and expressed as geometric standard deviation.

## RESULTS AND DISCUSSION

### Rational Design of *para*-Benzylamine Derivatives.

While the field of KLK's inhibitor discovery is relatively underdeveloped despite very huge interest in several therapeutic areas, recent reviews highlight the interest and need for further works.<sup>24–28</sup>

A common approach for the development of inhibitors has been to use natural peptide inhibitors as starting points, exploiting combinatorial or designed mutations to achieve selectivity toward the targeted KLK (e.g., compound I, Chart 1).<sup>24,28</sup> However, the development of subtype-selective KLK inhibitors remains challenging. Papo and collaborators developed a yeast-displayed mutant library of the human

amyloid precursor protein Kunitz protease inhibitor (APPI) domain to derive serine protease inhibitors especially of KLK6.<sup>29</sup> Recently, Miller and co-workers have reported decapeptides as potent KLK6's inhibitors to derive activity-based probes (compound II, Chart 1).<sup>30</sup> Our team has also recently identified 6-substituted coumarin-3-carboxylate derivatives as mechanism-based inhibitors (suicide substrates, compound III, Chart 1).<sup>31</sup> Several small molecules were also reported as reversible inhibitors of KLK6. Among them, benzamidine and benzylamine derivatives are probably the most potent inhibitors (e.g., compounds IV and V, Chart 1).<sup>32,33</sup> Especially, *N*-(4-aminomethyl-phenyl)-2-hydroxy-benzamide derivatives reported by Liang and co-workers are easily accessible and can be subjected to a large chemical diversification for structure–activity relationship (SAR) studies. Moreover, these compounds can potentially provide access to submicromolar inhibitors. In this study, nine analogues were described and the 5-*tert*-butyl derivative (compound V, Chart 1) revealed to be the most potent inhibitor of this series (half-maximal inhibitory concentration (IC<sub>50</sub>) = 0.3 μM) constituting an initial hit.<sup>33</sup> Substitution of the methylene group of the benzylamine as well as alkylation at the amino nitrogen led to inactive compounds, which clearly demonstrates that the amino group of the benzylamine is mandatory for the KLK6 inhibition. X-ray structure obtained with one of the derivatives of this series revealed that the benzylamine group bound into the S1 pocket of KLK6 by sharing a primary amine H-bonding with the side chain of N189. The side chain of I218 is also an important factor to the binding affinity through hydrophobic interaction with the phenyl ring of the benzylamine moiety. The hydroxyl group of the phenol occupied the center of the oxyanion hole, forming an H-bonding network with the backbone NH groups of G193 and S195 (Figure 1A,B). Keeping constant these key elements involved in KLK6 interaction (Figure 1C), we synthesized and evaluated novel series of *N*-(4-aminomethyl-phenyl)-2-hydroxy-benzamide and hydroxynaphthamide derivatives and identified druglike reversible organic inhibitors of KLK6 and its associated proteolytic network.

Targeted compounds, as well as the reference compound V (now named compound 28) were synthesized as reported in Scheme 2.

Briefly, compound 2 was obtained in two steps from 4-nitrobenzylamine hydrochloride after *tert*-butyloxycarbonyl (Boc) protection of the amine group, followed by the reduction of the nitro function. Compound 2 was then coupled with the appropriate salicylic or naphthoic acid in the presence of *N*-(3-dimethylaminopropyl)-*N'*-ethylcarbodiimide hydrochloride (EDCI) to offer compounds 3–25 in moderate yields. Compound 27 was synthesized by reductive amination with aldehyde 26 in the presence of sodium borohydride. Reaction between 1-naphthoic acid, 1-Boc-4-aminopiperidine and EDCI offered compound 52 in 64% yields. Finally, Boc group was removed using a mixture of hydrochloric acid in 1,4-dioxane to offer compounds 28–51 and 53 as hydrochloride salts.

**Inhibitory Potency Hit Compounds on KLK6 and on Its Proteolytic Network.** Newly synthesized compounds 28–51 and 53 were first screened on KLK6 through the evaluation of the percentage inhibition at 10 μM. This allows highlighting the promising compounds for the inhibition of KLK6. Among the 25 designed compounds, we preselected those raising an inhibition of at least 50% of the activity of

KLK6 at a concentration of 10 μM and then determined their inhibitory potency through the quantification of IC<sub>50</sub>.

Starting from reference compound 28 (Table 1) previously identified by Liang et al.,<sup>33</sup> several modifications were studied in the phenol series, to determine key structural elements for KLK6 inhibition. Suppression of the carbonyl group (compound 29) as well as the *tert*-butyl group (compound 30) led to the loss of the activity. Then, sensitivity to the position of the substituent carried out by the phenol group was observed in the methyl series (compounds 31–34). Substitution of position 4 and position 5, to a less extent, was most favorable to observe an optimal inhibition of KLK6. Several other groups were then introduced into C4 and C5. These positions must be substituted by an apolar or bulky group such as an isopropyl (compound 37) or a methyl group (compound 32) for C4-substituted derivatives and a *tert*-butyl group (compound 28) for C5-substituted derivatives. Interestingly, the substitution of the C5 position by a halogen (compound 35) or by a methoxy group (compound 36) is strongly unfavorable for the inhibition of KLK6.

When the inhibitor contains a naphthol group, a slight sensitivity with respect to the position of the hydroxyl group is observed. Indeed, it must be substituted at positions 1 or 3 for optimal inhibition of KLK6 (compounds 40 and 42, respectively). More generally, the hydroxyl group is essential because the inhibition of KLK6 decreases drastically when the inhibitor contains a naphthyl (compound 43) instead of a naphthol. This result is not surprising because, in the phenol series, the hydroxyl group was reported to be involved in key interactions notably with the S195 residue of KLK6. There is also a lack of inhibitory effect when the compound contains an indolyl (compound 44) or an oxoquinoline ring (compound 45) in place of the naphthol ring, indicating that the hydroxyl group could not be replaced by another hydrogen donor or acceptor (NH or ketone). Moreover, we noted the importance of the benzylamine group. Indeed, we observed a significant decrease in the inhibition when this same position is occupied by a piperidinyl group (compound 53). Finally, several substitutions into the naphthol ring were studied (compounds 47–51, see the Supporting Information (SI)). However, all studied modifications led to autofluorescent compounds that could not be evaluated, except when a methoxy group was introduced on position 6 (compound 47). In this case, a slight loss of activity compared to its unsubstituted analogue (compound 40) was observed.

Thus, among the newly synthesized compounds, five new hits were identified in the series of *para*-aminobenzyl compounds (molecules 32, 37, 40, 42, and 47) (Table 1), displaying IC<sub>50</sub> equal or below 5 μM. The IC<sub>50</sub> accounts for the effectiveness of the inhibitor with respect to the enzyme and allows a prioritization according to the inhibitory power. The IC<sub>50</sub> values place compounds 32 and 42 at the top, while reference compound 28 (IC<sub>50</sub> = 9.06 μM) has one of the lowest efficacies with respect to KLK6 among the selected inhibitors.

Then, we assessed the inhibitory potency of our hit compounds (32, 37, 40, 42, and 47) and of reference compound 28 toward KLK1 and plasmin, as these two proteases are thought to be part of the proteolytic network of KLK6 in MS.<sup>19</sup> All of these *para*-aminobenzyl derivatives lead to at least 50% inhibition of the plasmin activity except inhibitor 28 (45%) while all of the tested inhibitors lead to an inhibition of at least 50% of KLK1 activity at a concentration

Table 2. Efficacy of KLK6 *para*-Aminobenzyl Hit Inhibitors on Plasmin and KLK1<sup>a</sup>

Compound	Ar	X	IC <sub>50</sub> (μM)	
			Plasmin	KLK1
28	5- <i>tert</i> -butyl-2-hydroxyphenyl	CO	21.3 ± 3.6	38.6 ± 1.9
32	4-methyl-2-Hydroxyphenyl	CO	9.2 ± 0.6	26.3 ± 1.1
37	4-isopropyl-2-Hydroxyphenyl	CO	4.8 ± 0.2	8.4 ± 0.3
40	1-hydroxy-2-Naphthyl	CO	10.2 ± 0.6	21.3 ± 1.6
42	3-hydroxy-2-Naphthyl	CO	7.4 ± 0.6	5.1 ± 0.2
47	6-methoxy-1-hydroxy-2-naphthyl	CO	3.3 ± 0.2	16.1 ± 0.4
49	7-methyl-1-hydroxy-2-naphthyl	CO	6.7 ± 0.6	49.4 ± 4

<sup>a</sup>For each compound, the inhibitory effect was quantified by the IC<sub>50</sub>. To determine IC<sub>50</sub>, compounds at different concentrations (from 100 to 1.56 μM) are preincubated for 15 min at 37 °C with plasmin (3 nM) or KLK1 (0.75 nM) in 50 mM Tris buffer, 1 M citrate 0.05% Brij-35; pH 7.4 at 37 °C. The enzymatic reaction is then triggered by the addition of the Boc-QAR-AMC substrate (100 μM) for plasmin and H-PFR-AMC substrate (100 μM) for KLK1. The data result from at least three independent experiments in duplicate. The IC<sub>50</sub> values were calculated by fitting the experimental data to eq 2a or eq 2b and expressed as geometric standard deviation.

of 10 μM (data not shown). The inhibitory potency (IC<sub>50</sub>) of hit compounds was then determined. The IC<sub>50</sub> values with respect to plasmin place compound 47 (IC<sub>50</sub> = 3.3 μM) at the top while reference compound 28 (IC<sub>50</sub> = 21.3 μM) has one of the lowest efficiencies (Table 2). At the same time, compound 42 is characterized by an IC<sub>50</sub> value of 5.1 μM toward KLK1, while other compounds showed lower inhibitory potency and were thus not selected for further mechanistic studies (Table 2).

Hit compounds (32, 37, 40, 42, 47, 49) and reference compound 28 were assessed by the evaluation of their selectivity spectrum against a set of serine proteases and proteases involved in CNS homeostasis. Table 3 provides an overview of putative cross-inhibition within a large set of proteases, both serine proteases challenging in the CNS (KLK8, tissue-type plasminogen activator (tPA), thrombin, trypsin, trypsin-3, KLK11) and other kallikreins (KLK3, KLK4, KLK5, KLK14), matriptase, and diverse proteases involved in CNS inflammation (caspase-2, caspase-3, caspase-6, cathepsin L). Overall, this screening shows that hit compounds 32 and 42 have little effect on these selected challenging proteases in

contrast to the other identified inhibitors (28, 37, 40, 47, 49) that display significant inhibition on several proteases. This allows us to conclude that compounds 32 and 42 are quite specific to KLK6 and its proximal proteolytic network.

**Mechanism of Inhibition: Hit Compounds.** Mechanistic studies were only performed for hit compound that display an ideal balance between potency and selectivity profiles toward KLK6 and its proximal proteolytic network (KLK1 and plasmin) as well as the reference compound 28 for comparison. The reversibility of the inhibitions exerted by the compounds on KLK6 and its proteolytic network (plasmin and KLK1) were demonstrated by the dilution method as described in the Experimental Section. This experiment distinguishes an irreversible covalent inhibitor from a reversible one. Whatever the compound tested, a 1/100 dilution of the enzyme–inhibitor complex allowed restoring the initial activity of KLK6 to more than 80%. Hence, hit compounds are reversible inhibitors (Figure 2). The mechanisms were determined using representations of Dixon for hits and reference compounds. The results are shown in Figure 2. The Dixon graphs obtained for compounds 28, 32, and 40

Table 3. Selectivity of the Inhibition of Hit Compounds toward Selected CNS Concurrent Proteases (Inhibition Percentage at 10  $\mu\text{M}$ , %)<sup>a</sup>

Inhibitor Protease	28	32	37	40	42	47	49
KLK4	0	0	45	14	2	3	6
KLK5	35	5	24	22	4	31	0
KLK7	9	12	7	0	6	10	11
KLK8 <sup>b</sup>	16	34	58	22	61	45	53
KLK11 <sup>b</sup>	56	39	75	80	45	0	88
KLK13	5	10	15	2	19	0	12
KLK14	1.5	3	12	11	5	16	4
Caspase-2 <sup>b</sup>	5	0	15	30	4	14	8
Caspase-3	11	0	13	10	5	3	10
Caspase-6 <sup>b</sup>	13	5	12	56	40	70	31
Cathepsin L <sup>b</sup>	20	32	1	30	25	28	27
Matriptase	0	0	13	29	8	37	0
Thrombin	2	0	32	5	0	6	6
tPA	11	0	6	18	6	10	9
Trypsin	5	15	91	34	25	41	32
Trypsin 3 <sup>b</sup>	15	20	73	30	36	32	21

<sup>a</sup>Each inhibitor (10  $\mu\text{M}$ ) is preincubated with the enzyme at the optimal concentration for 15 min at 37 °C. The reaction is triggered by the addition of the specific 7-amino-4-methylcoumarin (AMC) substrate in the appropriate buffer (see the Selectivity Profiling section). The data result from at least three independent experiments with a standard deviation <10%. <sup>b</sup>Proteases implicated in the CNS physiological processes. Gray light: significant percentage of inhibition.

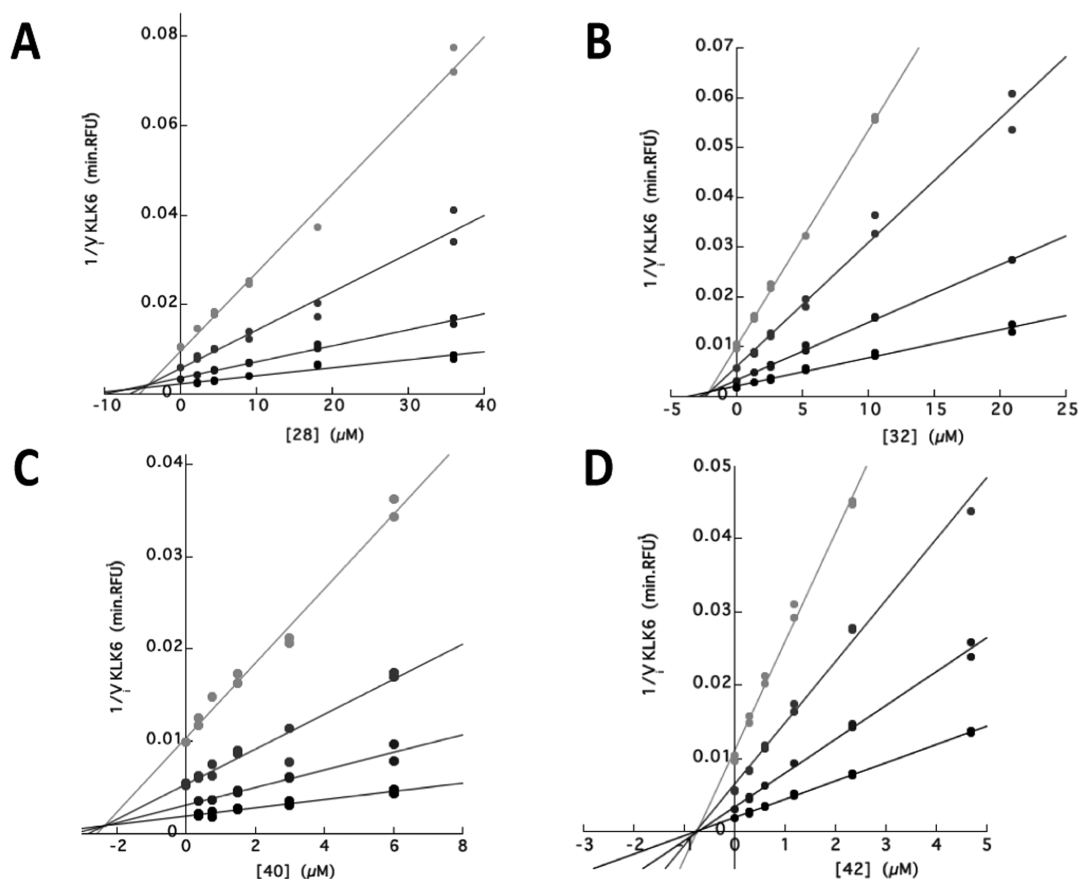
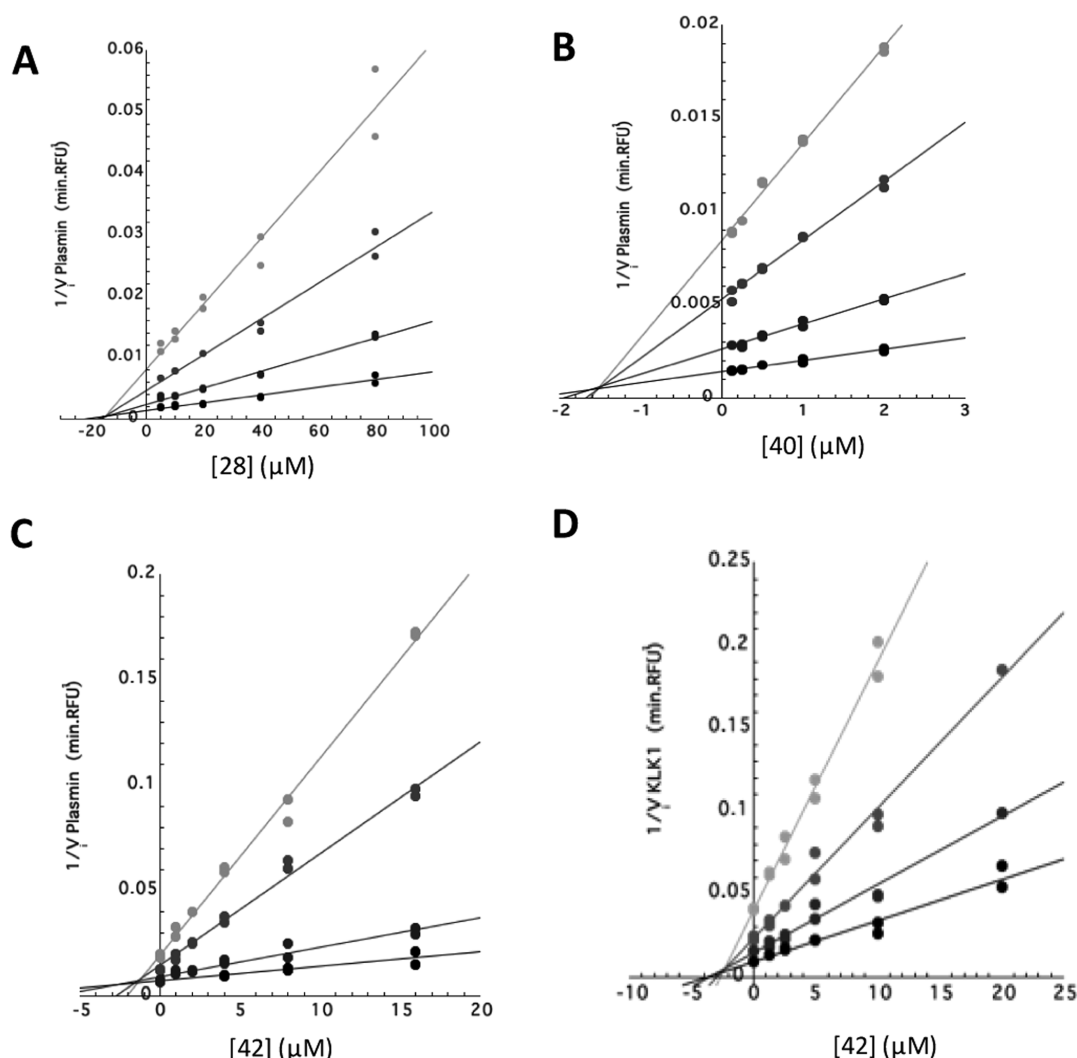


Figure 2. Mechanisms of inhibition toward KLK6. Dixon plots for inhibitors 28 (A), 32 (B), 40 (C), and 42 (D). Inhibitors at different concentrations (1/4; 1/2; 1; 2; 4 of the  $\text{IC}_{50}$  value) were tested using 2 nM KLK6 with substrate Boc-QAR-AMC at different concentrations (125; 62.5; 31.25; 15.625  $\mu\text{M}$ ) in 50 mM Tris, 1 M citrate, 0.05% Brij-35, pH 7 buffer at 37 °C.



**Figure 3.** Mechanisms of inhibition toward KLK1 and plasmin. Dixon plots for inhibitors 28 (A), 40 (B), and 42 (C) toward plasmin. (D) Dixon plot for inhibitor 42 toward KLK1. Inhibitors at concentrations (1/4; 1/2; 1; 2; 4 of the  $IC_{50}$  value) were tested on plasmin (3 nM) or KLK1 (0.75 nM) with, respectively, Boc-QAR-AMC or H-PFR-AMC substrates at concentrations (125; 62.5; 31.25; 15.625  $\mu$ M) in 50 mM Tris buffer, 1 M citrate, 0.05% Brij-35, pH 7 at 37 °C.

**Table 4. Mechanisms of Inhibition and  $K_i$  Values of Hit Compounds on KLK6 and Its Associated Proteolytic Network (KLK1 and Plasmin)<sup>a</sup>**

compound	KLK6		plasmin		KLK1	
	type of inhibition	$K_i$ ( $\mu$ M)	type of inhibition	$K_i$ ( $\mu$ M)	type of inhibition	$K_i$ ( $\mu$ M)
28	competitive	4.3 $\pm$ 1.6	competitive	14.5 $\pm$ 1.2	NA	NA
32	competitive	2 $\pm$ 0.5	NA	NA	NA	NA
37	competitive	1.5 $\pm$ 0.2	NA	NA	NA	NA
40	competitive	2.4 $\pm$ 0.1	competitive	1.5 $\pm$ 0.5	NA	NA
42	noncompetitive	0.8 $\pm$ 0.3	competitive	1.3 $\pm$ 0.53	competitive	2.4 $\pm$ 0.5
47	competitive	1 $\pm$ 0.3	NA	NA	NA	NA

<sup>a</sup>NA, not applicable.

(Figure 2A–C) are typical of competitive inhibitors. Compounds 28, 32, and 40 have  $K_i$  values of 4.3, 2, and 2.4  $\mu$ M, respectively. Surprisingly the mechanistic profile of compound 42 was found compatible with a noncompetitive inhibition with a  $K_i$  value of 0.8  $\mu$ M which may be indicative of a more complex binding (Figure 2D). The Dixon plots for compounds 37 and 47 are provided in the Supporting Information (Figure S1).

Concerning plasmin and KLK1, all compounds are reversible inhibitors as shown using the dilution method. Dixon plots obtained for compounds 28, 40, and 42 (Figure 3A–C) are typical of competitive inhibitors toward plasmin. Compounds 28, 40, and 42 have  $K_i$  values of 14.5, 1.5, and 1.3  $\mu$ M, respectively. The Dixon plot for KLK1 obtained with inhibitor 42 is also typical of a competitive inhibitor ( $K_i = 2.4 \mu$ M) (Figure 3D and Table 4). Hence, it is shown that some of



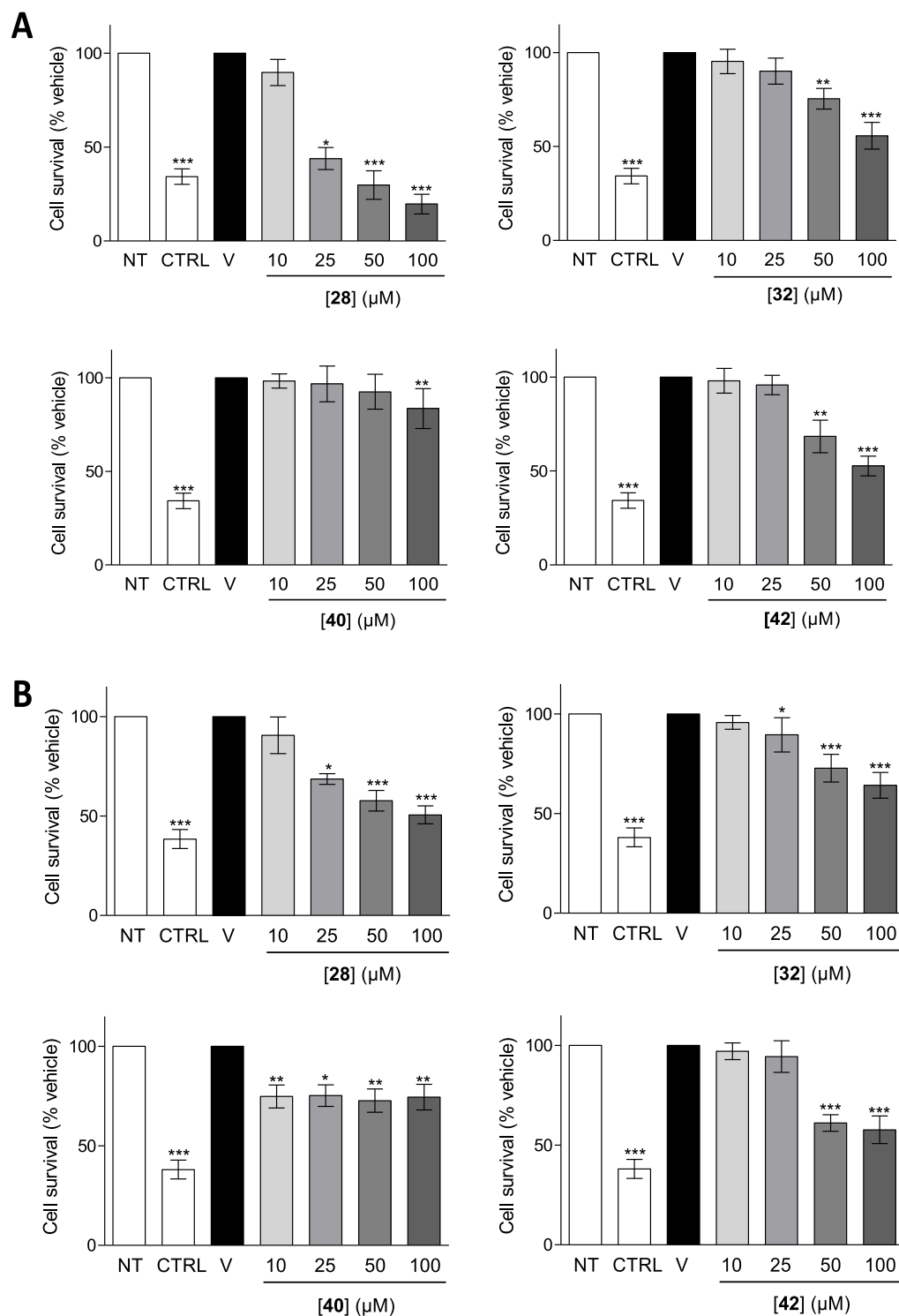


**Figure 4.** Cytotoxicity of hit inhibitors (**32**, **40**, and **42**) and reference compound **28** against primary cultures of cortical and striatal neurons. (A) Cortical neurons. (B) Striatal neurons. Primary cultures were treated with inhibitors in a concentration range from 10 to 100  $\mu\text{M}$ , with the vehicle (dimethyl sulfoxide (DMSO) 1%, "V"), or with rotenone 50  $\mu\text{M}$  (CTRL) for 24 h ( $N = 3$ ). Cell survival was then measured using XTT assay. All data sets were compared to the vehicle condition (V) for the generation of the  $p$ -values. \* $p$ -value < 0.05; \*\* $p$ -value < 0.01; \*\*\* $p$ -value < 0.001 (Kruskal–Wallis test). NT: no treatment.

our hit KLK6 inhibitors also target key serine proteases of KLK6 proteolytic network with a relatively good affinity, which may constitute an interesting perspective for a polypharmacological strategy.

**Evaluation of the Cytotoxicity of Hit Compounds toward Neural Cells.** To ensure that hit compounds (**32**, **40**,

and **42**) may constitute good starting points for further applications, their potential cytotoxicity toward neural cells was first evaluated in comparison to reference compound **28** on primary cultures of mouse cortical and striatal neurons at 10, 25, 50, and 100  $\mu\text{M}$  (Figure 4A). Compounds **32** and **42** showed similar effects on both cortical and striatal neurons. A

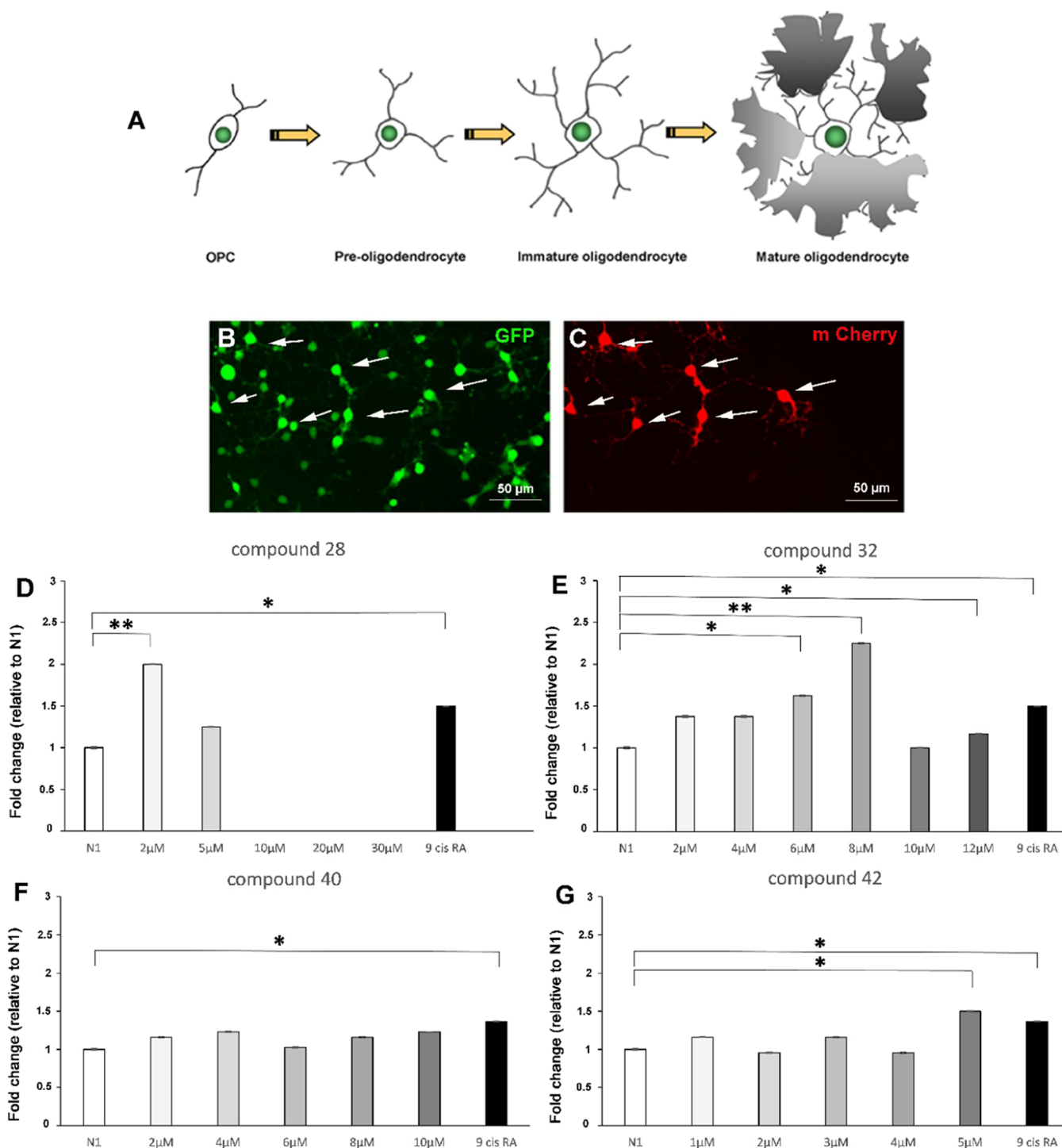


**Figure 5.** KLK6 inhibitors promote oligodendrocyte differentiation on the CG4 mCherry/GFP cell line. Schematic representation of the different developmental stages of the CG4 cell line (A). Differentiation of the mCherry/GFP double-fluorescent CG4 cell line, after 4 days of differentiation in basal medium (B, C). GFP fluorescence is shown in (B) and mCherry fluorescence in (C). Note that the differentiation of CG4 cells is not synchronous in these cultures and the expression of mCherry occurs specifically at the mature oligodendrocyte stage. Graphs of the fold change of the number of mCherry+ cells in N1 alone, N1 + compound 28 (D), N1 + compound 32 (E), N1 + compound 40 (F), or N1 + compound 42 (G), after 4 days of differentiation. The treatment with KLK6 inhibitors 32 and 42 induces a significant increase of CG4 cell differentiation at 8 and 5  $\mu$ M, respectively, relative to the N1 basal medium. Note that CG4 cells treated with compound 28 at 2  $\mu$ M lead to a significant increase in the number of mCherry+ oligodendrocytes. However, at higher concentrations with this compound (ranging from 10 to 30  $\mu$ M), cells were lost presumably due to a cytotoxicity. Wilcoxon–Mann–Whitney test: \* $p \leq 0.05$ , \*\* $p \leq 0.01$ . 9-*cis*-retinoic acid (9-*cis*-RA, 1  $\mu$ M) was used as a positive control. Scale bar (B, C): 50  $\mu$ m.

slight effect is observed from a concentration of 50  $\mu$ M of inhibitors 32 and 42, with percentages of cell survival around 65–70%. In contrast, compound 40 is the only compound

showing a cytotoxic effect on striatal neurons from a concentration of 10  $\mu$ M, this cytotoxicity is stable over the concentration range, meaning that a plateau may be reached

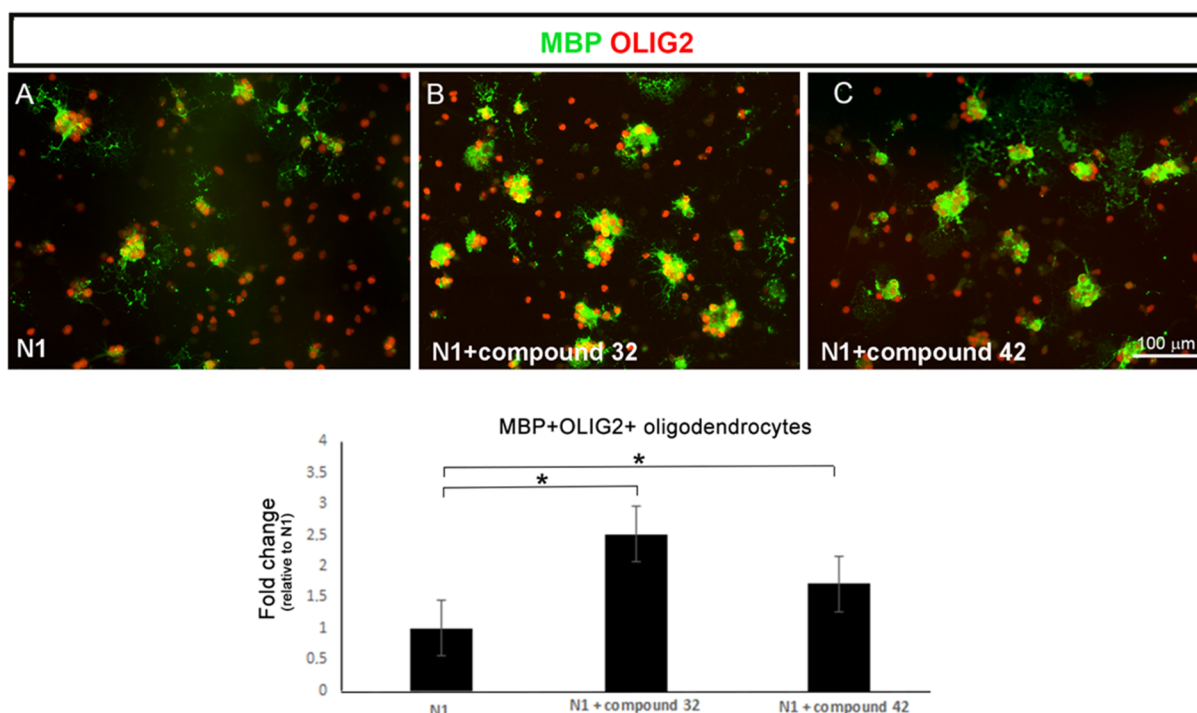


**Figure 6.** KLK6 inhibitors promote oligodendrocyte differentiation of primary OPC cultures. Primary OPC cultures, stained for MBP (green) and Olig2 (red), after 4 days of differentiation in basal medium (A), in the presence of compound 42 ((B) 5  $\mu$ M) or compound 32 ((C) 8  $\mu$ M). The treatment with KLK6 inhibitors induces a significant increase of MBP+ oligodendrocytes with respect to control.  $N = 3$  independent experiments; Wilcoxon–Mann–Whitney test:  $*p \leq 0.05$ . Scale bar (A–C): 100  $\mu$ m.

(Figure 4B). Thus, these newly identified inhibitors are all very poorly cytotoxic in comparison to the reference inhibitor 28, which displays a noticeable cytotoxic effect, even at 25  $\mu$ M, very close to the treatment with rotenone vehicle at 50  $\mu$ M.

Hence, since compounds 32, 40, and 42 did not show toxic effects toward neurons, they were selected for further studies in oligodendrocyte precursor cell (OPC) cultures as a relevant biological model for MS.

**Pro-differentiating Effect of Hit Compounds.** Oligodendrocytes are derived from OPCs, a class of progenitors highly abundant during development but also persistent in the adult CNS, where they contribute to myelin remodeling and remyelination following acute demyelination. Although efficient remyelination occurs in the early stages of MS, it becomes inefficient and ultimately fails with disease progression. Remyelination requires the generation of new mature oligodendrocytes (OLs) from OPCs that must be recruited to the demyelinated lesions. Over the last decade, there has been huge interest in developing medicines to improve remyelination in MS.<sup>34</sup> The approaches range widely, from developing novel medicines and repurposing existing drugs. We thus assayed hit compounds on CG4 cell line and rat OPC primary cultures to check for their ability to induce differentiation. To monitor OPC differentiation, we developed a stable CG4 cell line expressing the green fluorescent protein (GFP) reporter at all stages of the oligodendroglial lineage cells and the mCherry reporter only in mature oligodendrocytes (Figure 5A). This innovative cellular assay allows the screening of pro-myelinating compounds based on the detection of fluorescence parameters. Indeed, both morphological changes and generation of mature oligodendrocytes can be monitored in a single assay, based on enhanced GFP (EGFP) and mCherry fluorescence, respectively. After few days in basal medium,

CG4 cells start to differentiate and expressed mCherry (Figure 5B,C). Fluorescence imaging (90 image fields were acquired for each condition) and quantification were performed with the ArrayScan XTI Imaging System. For each concentration tested, we quantified the number of mCherry+ cells and data were normalized relative to control (N1 basal medium). 9-*cis*-Retinoic acid (9-*cis*-RA), a well-known compound promoting OPC differentiation was used a positive control.<sup>53</sup>

Our data revealed no statistically significant change in the number of mCherry+ cells after treatments with compounds 40 (Figure 5F). For compound 28, a significant increase in the number of mCherry+ oligodendrocytes was observed at 2  $\mu$ M, while treatments at higher concentrations ranging from 10 to 30  $\mu$ M lead to a complete loss of cells (Figure 5D), presumably due to cytotoxicity. In contrast, for compound 32 (Figure 5E) a significant increase of differentiation was observed with respect to basal control at concentrations of 6  $\mu$ M ( $p \leq 0.05$ ) and 8  $\mu$ M ( $p \leq 0.01$ , Mann–Whitney test), and for compound 42 (Figure 5G) at 5  $\mu$ M ( $p \leq 0.05$ , Mann–Whitney test). Thus, compounds 32 and 42 promote the differentiation of CG4 cells into mature oligodendrocytes. In view of their pharmacological and biological profiles, compounds 32 and 42 appear particularly suitable. Compounds 32 and 42 were also evaluated on primary cultures of rat OPCs (Figure 6). In this model, the differentiation rate was measured by the quantification of the number of MBP-expressing oligodendrocytes. MBP is a major constituent of myelin and is commonly used as a marker of mature oligodendrocytes. Compounds 32 and 42 promote the differentiation at concentrations of 8 and 5  $\mu$ M, respectively. Overall, these findings support the pro-myelinating potential of *para*-aminobenzyl-hit derivatives.

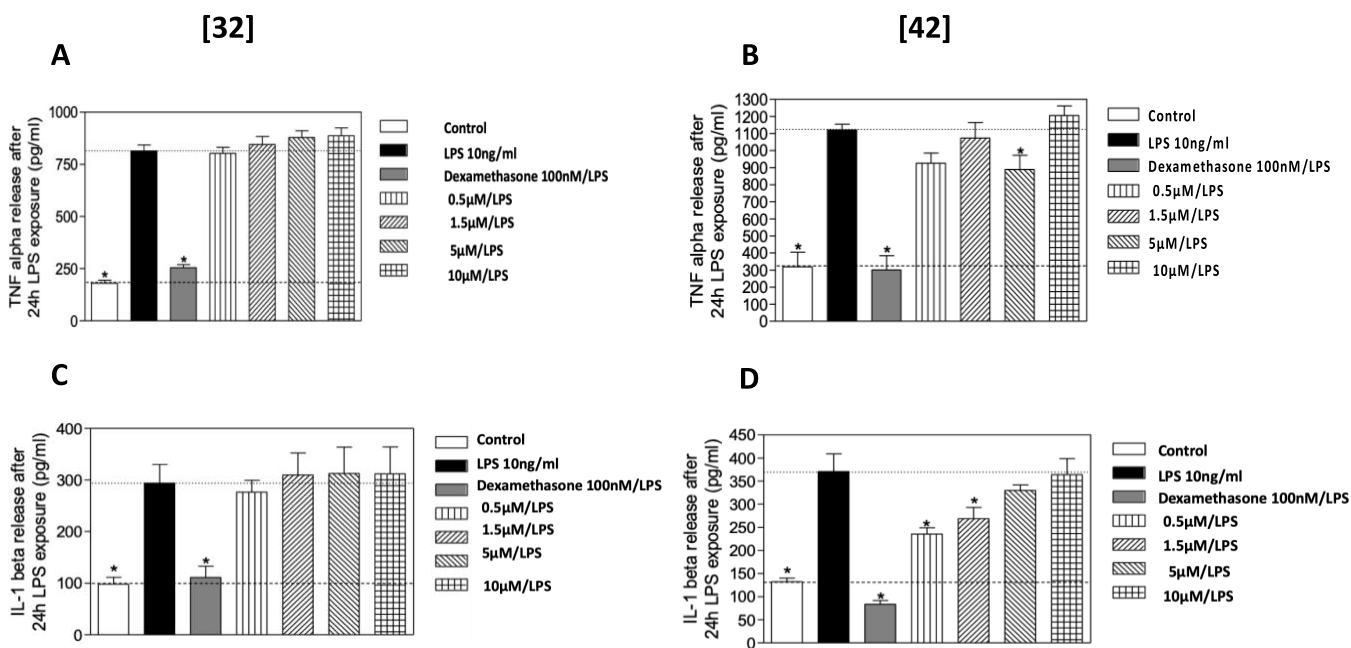


**Figure 7.** Anti-inflammatory potential of KLK6 inhibitors on a primary culture of microglia. Changes in TNF- $\alpha$  (A, B) and IL-1 $\beta$  (C, D) secretions after 24 h of LPS exposure (10 ng/mL) and treatment by either inhibitor 32 (left) or 42 (right) in the concentration range [0.5–10  $\mu$ M]. Cytokine secretion was measured by enzyme-linked immunosorbent assay (ELISA). The treatment with inhibitor 42 induces a significant decrease of TNF $\alpha$  and IL1- $\beta$  secretions. Control: no treatment. Dexamethasone (100 nM): positive control ( $n = 3$ ) (graph,  $*p \leq 0.05$ ).

**Anti-inflammatory Properties of Hit Compounds.** In MS, chronic activation of microglia may contribute to neurodegeneration and neuroinflammation.<sup>35</sup> Thus, we also examined the impact of hit compounds 32 and 42 on microglial activation and proinflammatory cytokines. These experiments were carried out in primary microglial cells isolated from newborn rat brain.<sup>36</sup> Effects of selected compounds on microglia were analyzed after treatment with lipopolysaccharide (LPS, 10 ng/mL) alone or in the presence of different concentrations framing IC<sub>50</sub> values of compounds 32 and 42, using dexamethasone as a positive control (Figure 7). Using quantitative reverse transcription polymerase chain reaction (RT-qPCR) of pro- and anti-inflammatory cytokine gene expression, we showed that compound 42 significantly lowered the expression of tumor necrosis factor (TNF) $\alpha$  and interleukin (IL)-1 $\beta$  proinflammatory cytokines while compound 32 had no effect. This result illustrates potential distinct dual therapeutical effects and/or mechanism of action for these hit compounds.

**Molecular Docking Modeling to the Study Structural Basis of the Inhibition.** *In silico* analyses using molecular docking with the AutoDock Vina software highlighted some characteristic structural bases on the inhibition of hit compounds 42 and 32 (Figure 8A). Figure 8B,C illustrates their positioning for the best docking poses. Overall, the orientation of both compounds within the active site is identical with the benzylamine group pointing to the S1 pocket and the phenol/naphthol groups to the catalytic triad. Inhibitors 32 (Figure 8B) and 42 (Figure 8A) share several polar contacts with some active site residues, namely, H57 and S195. In particular, the NH of the amide bond of compound 32 establishes a direct H-bond with the catalytic S195. We do not exclude a certain flexibility in this region, given the obtained results, which could allow the NH of the amide bond of compound 42 to behave similarly, this behavior may in part explain the noncompetitive mechanism underlined by Dixon

plots. The OH hydroxyl group of phenols or naphthols could also contribute to a polar bond with Q192 side chain as well as the NH backbone of G193. Finally, the primary amine shows strong polar contact in both cases with D189 and S190 side chains and with W215 backbone. The visual inspection of other docking poses with lower scores informed us about the certain degree of freedom (dof) of the benzylamine moiety inside the S1 pocket, the benzyl group having enough space to slightly rotate around its axis, even suggested by the two best poses of compounds 32 and 42. These poses are quite compatible with their mechanism of inhibition.

**Pharmacological Profile and Evaluation of Druglike Properties.** To gain more insights on the druglike potential of the two selected hit compounds, different evaluations were performed to assess their: (i) their putative effect on coagulation; (ii) their cross-reactivity toward key pharmacological targets using the SafetyScreen44 Panel from Eurofins;<sup>37</sup> (iii) some absorption, distribution, metabolism, excretion, and toxicity (ADME-Tox) properties: solution properties (aqueous solubility in simulated fluids and plasma protein binding), *in vitro* absorption (Caco2 cell line); *in vitro* metabolism (intrinsic clearance using human liver microsomes). More relevant parameters are summarized in Table S2, Supporting Information. Altogether, these evaluations demonstrated that hit compounds 32 and 42 bear a very favorable pharmacological profile. They were shown to have no toxicity on coagulation after incubation with human blood (neither the activated partial thromboplastin time nor the prothrombin ratio was modified) and to possess acceptable aqueous solubility (>150  $\mu$ M, except for 42 at pH  $\geq 7.4$ ), permeability (>90%), and clearance properties (half-life >120 min) compared to reference substances. Interestingly, among the 44 screened targets, both receptors and enzymes, very few were inhibited by our lead compounds. No activity at ion channels (including human ether-à-go-go-related gene (hERG)) was detected meaning weak toxicity. The only significant detected

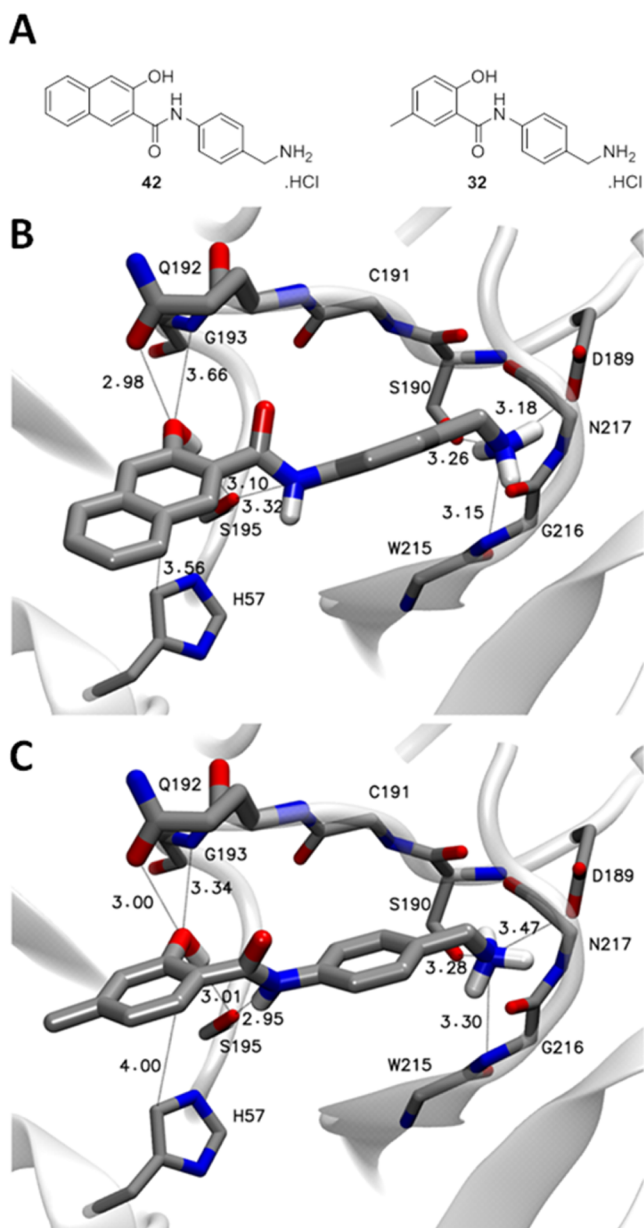


**Figure 8.** Structure of lead compounds 42 and 32 (A) and pose predictions by molecular docking of 42 (B) and 32 (C) in KLK6. Most relevant interactions were depicted by dashed lines together with distances in angstrom. Compounds as well as residues of the proteins mainly involved in ligand interactions are shown in licorice, while the full proteins are shown in transparent-white cartoon. The color code for the atoms is as follows: carbon in gray, oxygen in red, nitrogen in blue, and hydrogen in white. The side chains that make no contact with 42 and 32, as well as hydrogens of the protein and nonpolar hydrogens of 42 and 32 were not represented for clarity.

off-targets were of interest for both CNS diseases (5-HT<sub>2A/2B</sub> serotonin receptors) and inflammation (COX-2).<sup>38</sup> Hence, the selected compounds display favorable druglike properties and thus constitute excellent starting point to derive drugs for regenerative therapy of MS and related diseases associated with a deregulation of KLK6 and proximal proteolytic network.

## CONCLUSIONS

Current MS therapeutics are mainly immunomodulatory, having very less effect on the neuro-regeneration of damaged

CNS tissue; they are thus primarily effective at the acute stage of disease, but much less so at the chronic stage. An MS therapy that has both immunomodulatory and neuro-regenerative effects would be highly beneficial. Novel targets aiming to promote such therapeutic strategies are thus of great interest.<sup>8</sup> KLK6 and its proximal proteolytic network may constitute a new opportunity to develop new therapeutics or molecular tools for MS pathophysiology. A series of *para*-aminobenzyl derivatives incorporating a phenol or a naphthol group was thus designed, synthesized, and studied for their properties to inhibit KLK6 activity and proteases that may be involved in the KLK6's pathological network in MS, namely, inhibitions of both KLK1 and plasmin may be interesting in a polypharmacological perspective.

Several designed low-molecular-weight inhibitors are low-micromolar potency and reversible toward KLK6. In the phenol series, introduction of an alkyl group at the C4 position led to more potent compounds (32 and 37), whereas in the naphthol series, the best activity was obtained with the 1- and 3-naphthol derivatives (40 and 42). Interestingly, these hit compounds were selective of KLK6 and its associated network over a large set of CNS concurrent proteases, and devoid of cytotoxic effects on primary cultures of mouse cortical and striatal neurons and oligodendrocytes. Most importantly, we show for the first time that synthetic inhibitors of KLK6 and proximal proteolytic network, a key actor of MS pathophysiology, are able to promote the differentiation of OPCs into mature oligodendrocytes *in vitro*, which is as far as we know the first report of such properties. Indeed, the presence of oligodendrocyte progenitors (OPCs) in the adult CNS, which are able to migrate and regenerate remyelinating oligodendrocytes in demyelinating lesions, represents the main cellular target for the development of pharmacological strategy aiming to promote remyelination. In line with this idea, compounds 32 and 42 were also tested for their potential effect on neuroinflammation using primary cultures of microglia. Compound 42 decreased significantly the expression of proinflammatory cytokines. Hence, compound 42 in contrast to compound 32 appears to be a good candidate as a first-in-class KLK6 inhibitor bearing both remyelinating and anti-inflammatory potentials. There is a growing interest to decipher mechanisms regulating OPC differentiation for the identification of novel specific pharmacological targets for remyelination-enhancing therapy.<sup>34</sup> On the other hand, there also a growing interest for pro-differentiating compounds selected first through screening campaigns and more recently using rational design as illustrated in up-to-date reports. Namely, spiroindolines were shown as novel inducers of OPC differentiation.<sup>39</sup> Recently, benzothiazoles LRRK2 inhibitors were shown to promote OPC proliferation and differentiation through Wnt/ $\beta$ -catenin signaling pathway.<sup>40</sup> Moreover, modified flavonoids were reported as selective inhibitors of hyaluronidase activity and could promote OPC maturation, making them excellent candidates to accelerate myelination or promote remyelination following perinatal and adult CNS insults.<sup>41</sup> Thus, in view of their pharmacological and biological properties, *para*-aminobenzylamine derivatives 32 and 42 appear particularly valuable starting points for the development of original pharmacological strategies aiming to promote remyelination in demyelinating diseases, such as MS.

## EXPERIMENTAL SECTION

All reagents were of analytical grade. Distilled water was filtered and deionized through a Millipore water purification system.

**Chemistry Materials and General Procedures.** Commercially available reagents and solvents were used without further purification. Reactions were monitored by an analytical Waters Alliance 2690 high-performance liquid chromatography (HPLC) instrument, equipped with a photodiode array and an analytical Chromolith SpeedROD RP-C18 185 Pm column (50 × 4.6 mm<sup>2</sup>, 5 mm), at a flow rate of 3.0 mL/min, and gradients of 100/0 to 0/100 eluents A/B for 5 min (eluent A = H<sub>2</sub>O/0.1% trifluoroacetic acid (TFA) and B = CH<sub>3</sub>CN/0.1% TFA). Detection was performed at 214 nm. <sup>1</sup>H and <sup>13</sup>C NMR spectra were recorded on Bruker spectrometers (300 or 400 MHz) at room temperature in deuterated solvents. Chemical shifts (δ) are expressed in parts per million (ppm), relative to the resonance of CDCl<sub>3</sub> = 7.26 ppm for <sup>1</sup>H (77.16 ppm for <sup>13</sup>C), CD<sub>3</sub>OD = 3.31 ppm for <sup>1</sup>H (49.00 ppm for <sup>13</sup>C) or DMSO-*d*<sub>6</sub> = 2.50 ppm for <sup>1</sup>H (39.52 ppm for <sup>13</sup>C). The following abbreviations were used: singlet (s), doublet (d), triplet (t), quartet (q), multiplet (m), broad singlet (bs). Analytical thin-layer chromatography (TLC) was carried out on aluminum plates covered with 0.2 mm of silica, and column chromatography was performed on silica gel 60 (70–230 mesh).

The liquid chromatography/mass spectrometry (LC/MS) system consisted of a Waters Alliance 2695 HPLC, coupled to a Micromass (Manchester, U.K.) ZQ spectrometer (positive electrospray ionization mode, ESI+). All of the analyses were carried out using a Merck Chromolith SpeedROD C18, 25 × 4.6 mm<sup>2</sup> reversed-phase column. A flow rate of 3 mL/min and a gradient of 0–100% B over 3 min (or over 15 min) were used. Eluent A: water/0.1% HCO<sub>2</sub>H; eluent B: acetonitrile/0.1% HCO<sub>2</sub>H. Retention times (RT) are given in minutes. Nitrogen was used for both the nebulizing and drying gas. The data were obtained in a scan mode ranging from 100 to 1000 *m/z* in 0.1 s intervals; 10 scans were summed up to get the final spectrum. High-resolution mass spectrometry (HRMS) analyses were performed with a Waters Synapt G2-S time-of-flight mass spectrometer fitted with an electrospray ionization source. All measurements were performed in the positive ion mode. Melting points (mp) are uncorrected and were recorded on a Stuart capillary melting point apparatus SMP3. All compounds tested for biological activity showed >95% purity, as assessed by reversed-phase HPLC (RP-HPLC) (Chromolith SpeedROD RP-C18 185 Pm column 50 × 4.6 mm<sup>2</sup>, 5 μm; flow rate: 5.0 mL/min; gradients from 100/0 to 0/100 eluents A/B over 5 min, in which eluent A = H<sub>2</sub>O/0.1% TFA and B = CH<sub>3</sub>CN/0.1% TFA; detection was done at 214 nm).

Compound **26** was synthesized according to the procedure described by Darensbourg et al.<sup>42</sup> and its physical characteristics were in agreement with the published data. Carboxylic acids were commercially available or synthesized according to the procedures described in SI.

**Synthesis of tert-Butyl (4-Nitrobenzyl)carbamate (1).** To a solution of 4-nitrobenzylamine hydrochloride (1 g, 5.3 mmol) in 10 mL of dichloromethane were added 480 μL of triethylamine (348 mg, 3.44 mmol, 1.3 equiv) and 790 μL of tert-butyl dicarbonate (751 mg, 3.44 mmol, 1.3 equiv). The solution was stirred at room temperature for 2 h. Then, 0.3 equiv of aminomethyl polystyrene resin was added and the suspension was stirred for 1 h. After filtration, the solution was washed with 1 M aqueous potassium hydrogensulfate solution (2 × 15 mL) and brine (15 mL). The organic layer was dried over Na<sub>2</sub>SO<sub>4</sub>, filtered, and the solvent was evaporated *in vacuo* to offer compound **1** as a white solid (*m* = 1.06 g, 80% yield); mp 109–111 °C (lit. 109–110 °C);<sup>43</sup> <sup>1</sup>H NMR (CDCl<sub>3</sub>, 300 MHz): δ ppm 1.43 (s, 9H), 4.37 (d, 2H, *J* = 6.2 Hz), 5.03 (bs, 1H), 7.41 (d, 2H, *J* = 8.8 Hz), 8.14 (d, 2H, *J* = 8.8 Hz); <sup>13</sup>C NMR (CDCl<sub>3</sub>, 75 MHz): δ ppm 27.5, 44.2, 85.3, 123.9, 127.9, 146.9, 147.4, 156.0; HPLC, RT = 1.68 min.

**Synthesis of tert-Butyl (4-Aminobenzyl)carbamate (2).** To a solution of compound **1** (1 g, 4.0 mmol) in 20 mL of ethyl acetate was added 10% palladium activated on charcoal (~20 mg). The suspension was hydrogenated at atmospheric pressure for 4 h at room temperature. The suspension was then filtered on celite, and the

filtrate was evaporated under reduced pressure to yield compound **2** as a pale orange solid, *m* = 880 mg, quantitative yield; mp 72–75 °C (lit. 72–75 °C);<sup>44</sup> <sup>1</sup>H NMR (CDCl<sub>3</sub>, 300 MHz): δ ppm 1.43 (s, 9H), 3.60 (bs, 2H), 4.14 (d, 2H, *J* = 5.6 Hz), 4.74 (bs, 1H), 6.60 (d, 2H, *J* = 8.4 Hz), 7.02 (d, 2H, *J* = 8.4 Hz); <sup>13</sup>C NMR (CDCl<sub>3</sub>, 75 MHz): δ ppm 28.5, 44.5, 79.4, 115.3, 128.9, 135.1, 145.8, 155.9; HPLC, RT = 0.93 min; MS (ESI+): *m/z* 223.3 [M + H]<sup>+</sup>.

**General Procedure for the Synthesis of Compounds 3–28.** To a solution of 100 mg of compound **2** (0.45 mmol) in 2.5 mL of THF were added 1 equiv of the appropriate carboxylic acid derivative (0.45 mmol) and 103 mg of *N*-(3-dimethylaminopropyl)-*N'*-ethylcarbodiimide hydrochloride (1 equiv, 0.45 mmol). The solution was stirred at reflux for 12 h. After cooling to room temperature, the solution was evaporated to dryness. The crude product was dissolved in 20 mL of ethyl acetate, and the solution was washed with 1 N hydrochloric acid solution (3 × 20 mL) and then by 10% aqueous sodium carbonate solution. The organic layer was dried over Na<sub>2</sub>SO<sub>4</sub>, filtered, and the solvent was evaporated *in vacuo*. The resulting crude mixture was washed with Et<sub>2</sub>O for compounds **4**, **10**, and **23**. Compounds **13**, **16–21**, and **24** were used without further purification in the subsequent step. Other compounds were purified by chromatography on silica gel.

**tert-Butyl (4-(5-tert-Butyl-2-hydroxybenzoyl))-aminobenzylcarbamate (3).** Elution: DCM/EtOH 98.5/1.5 v/v; white solid (*m* = 58 mg, 32% yield); mp: 177–178 °C; <sup>1</sup>H NMR (CDCl<sub>3</sub>, 300 MHz): δ ppm 1.31 (s, 9H), 1.44 (s, 9H), 4.26 (d, 2H, *J* = 5.9 Hz), 4.89 (bs, 1H), 6.93 (d, 1H, *J* = 8.7 Hz), 7.24 (m, 2H), 7.48 (m, 4H), 8.24 (bs, 1H), 11.0 (s, 1H); <sup>13</sup>C NMR (CDCl<sub>3</sub>, 75 MHz): δ ppm 28.6, 31.4, 31.6, 44.4, 79.9, 114.4, 118.4, 121.9, 122.1, 128.2, 132.3, 136.0, 136.1, 142.0, 156.1, 159.3, 168.7; HPLC, RT = 2.10 min; MS (ESI+): *m/z* 399.3 [M + H]<sup>+</sup>; HRMS calcd for C<sub>23</sub>H<sub>31</sub>N<sub>2</sub>O<sub>4</sub> 399.2278, found 399.2272.

**tert-Butyl (4-(2-Hydroxybenzoyl))aminobenzylcarbamate (4).** White solid (*m* = 113 mg, 73% yield); mp: 107–171 °C; <sup>1</sup>H NMR (DMSO-*d*<sub>6</sub>, 300 MHz): δ ppm 1.40 (s, 9H), 3.30 (bs, 1H), 4.10 (d, 2H, *J* = 6.0 Hz), 6.96 (m, 2H), 7.23 (d, 2H, *J* = 8.4 Hz), 7.33 (bt, 1H, *J* = 6.0 Hz), 7.44 (td, 1H, *J* = 8.5, 1.6 Hz), 7.62 (d, 2H, *J* = 8.4 Hz), 7.97 (dd, 1H, *J* = 8.5, 1.6 Hz), 10.35 (s, 1H); <sup>13</sup>C NMR (DMSO-*d*<sub>6</sub>, 75 MHz): δ ppm 28.2, 43.0, 77.7, 117.2, 118.9, 120.9, 127.3, 128.9, 133.6, 136.0, 136.6, 155.7, 158.6, 166.5; HPLC, RT = 1.78 min; MS (ESI+): *m/z* 365.0 [M + Na]<sup>+</sup>, 287.1 [M + H - *t*-Bu]<sup>+</sup>; HRMS calcd for C<sub>19</sub>H<sub>23</sub>N<sub>2</sub>O<sub>4</sub> 343.1652, found 343.1655.

**tert-Butyl (4-(3-Methyl-2-hydroxybenzoyl))-aminobenzylcarbamate (5).** Elution: DCM/EtOH 92/2 v/v; light yellow solid (*m* = 125 mg, 78% yield); mp: 166.2–166.9 °C; <sup>1</sup>H NMR (CDCl<sub>3</sub>, 400 MHz): δ ppm 1.45 (s, 9H), 2.27 (s, 3H), 4.28 (d, 2H, *J* = 5.7 Hz), 4.85 (bs, 1H), 6.79 (t, 1H, *J* = 7.7 Hz), 7.28 (m, 3H), 7.37 (d, 1H, *J* = 7.7 Hz), 7.50 (d, 2H, *J* = 8.4 Hz), 8.00 (bs, 1H), 12.3 (s, 1H); <sup>13</sup>C NMR (CDCl<sub>3</sub>, 100 MHz): δ ppm 16.0, 28.6, 44.4, 79.9, 113.8, 118.4, 121.7, 123.1, 128.3, 128.4, 135.6, 136.1, 136.2, 156.1, 160.5, 169.1; HPLC, RT = 2.01 min; MS (ESI+): *m/z* 379.2 [M + Na]<sup>+</sup>, 301.2 [M + H - *t*-Bu]<sup>+</sup>; HRMS calcd for C<sub>20</sub>H<sub>25</sub>N<sub>2</sub>O<sub>4</sub> 357.1809, found 357.1811.

**tert-Butyl (4-(4-Methyl-2-hydroxybenzoyl))-aminobenzylcarbamate (6).** Elution: *n*-Hex/AcOEt 2/1 v/v; light yellow solid (*m* = 131 mg, 82% yield); mp: 191.8–192.8 °C; <sup>1</sup>H NMR (CDCl<sub>3</sub>, 400 MHz): δ ppm 1.45 (s, 9H), 2.33 (s, 3H), 4.28 (d, 2H, *J* = 5.5 Hz), 4.84 (bs, 1H), 6.70 (dd, 1H, *J* = 8.1, 1.1 Hz), 6.82 (d, 1H, *J* = 1.1 Hz), 7.27 (d, 2H, *J* = 8.4 Hz), 7.39 (d, 1H, *J* = 8.1 Hz), 7.50 (d, 2H, *J* = 8.4 Hz), 7.93 (bs, 1H), 11.94 (s, 1H); <sup>13</sup>C NMR (CDCl<sub>3</sub>, 100 MHz): δ ppm 21.9, 28.6, 44.4, 79.9, 112.1, 119.3, 120.3, 121.6, 125.5, 128.4, 136.1, 136.2, 146.1, 156.1, 162.1, 168.6; HPLC, RT = 1.90 min; MS (ESI+): *m/z* 357.2 [M + H]<sup>+</sup>, 379.1 [M + Na]<sup>+</sup>, 301.2 [M + H - *t*-Bu]<sup>+</sup>; HRMS calcd for C<sub>20</sub>H<sub>25</sub>N<sub>2</sub>O<sub>4</sub> 357.1809, found 357.1809.

**tert-Butyl (4-(5-Methyl-2-hydroxybenzoyl))-aminobenzylcarbamate (7).** Elution: *n*-Hex/AcOEt 2/1 v/v. Light yellow solid (*m* = 68 mg, 42% yield); mp: 174.5–175.5 °C; <sup>1</sup>H NMR (CDCl<sub>3</sub>, 400 MHz): δ ppm 1.45 (s, 9H), 2.32 (s, 3H), 4.28 (d, 2H, *J* = 5.4 Hz), 4.84 (bs, 1H), 6.91 (d, 1H, *J* = 8.4 Hz), 7.22–7.29 (m, 4H), 7.52 (d, 2H, *J* = 8.4 Hz), 7.96 (bs, 1H), 11.71 (s, 1H); <sup>13</sup>C NMR

(CDCl<sub>3</sub>, 100 MHz):  $\delta$  ppm 20.8, 28.6, 44.4, 79.9, 114.4, 115.5, 118.8, 121.6, 123.3, 125.7, 128.4, 135.8, 136.1, 156.1, 159.8, 168.6; HPLC, RT = 1.90 min; MS (ESI<sup>+</sup>):  $m/z$  379.2 [M + Na]<sup>+</sup>, 301.2 [M + H - *t*-Bu]<sup>+</sup>; HRMS calcd for C<sub>20</sub>H<sub>25</sub>N<sub>2</sub>O<sub>4</sub> 357.1809, found 357.1810.

**tert-Butyl (4-(6-Methyl-2-hydroxybenzoyl))-aminobenzylcarbamate (8).** Elution: *n*-Hex/AcOEt 2/1 v/v. Light yellow solid ( $m$  = 33 mg, 21% yield); mp: 149.0–150.0 °C; <sup>1</sup>H NMR (CDCl<sub>3</sub>, 300 MHz):  $\delta$  ppm 1.46 (s, 9H), 2.60 (s, 3H), 4.28 (d, 2H,  $J$  = 5.4 Hz), 4.91 (bs, 1H), 6.76 (d, 1H,  $J$  = 7.5 Hz), 6.84 (d, 1H,  $J$  = 8.2 Hz), 7.23 (dd, 1H,  $J$  = 8.2, 7.5 Hz), 7.27 (d, 2H,  $J$  = 8.0 Hz), 7.52 (d, 2H,  $J$  = 8.0 Hz), 7.72 (s, 1H), 9.85 (bs, 1H); <sup>13</sup>C NMR (CDCl<sub>3</sub>, 75 MHz):  $\delta$  ppm 22.1, 28.5, 44.3, 78.3, 115.7, 119.0, 121.0, 123.1, 128.4, 132.5, 135.5, 136.1, 136.2, 156.1, 159.2, 168.4; HPLC, RT = 1.60 min; MS (ESI<sup>+</sup>):  $m/z$  379.1 [M + Na]<sup>+</sup>, 301.2 [M + H - *t*-Bu]<sup>+</sup>; HRMS calcd for C<sub>20</sub>H<sub>25</sub>N<sub>2</sub>O<sub>4</sub> 357.1809, found 357.1808.

**tert-Butyl (4-(5-Bromo-2-hydroxybenzoyl))-aminobenzylcarbamate (9).** Elution: *n*-Hex/AcOEt 4/1 v/v; white solid ( $m$  = 24 mg, 12% yield); mp: >300 °C; <sup>1</sup>H NMR (DMSO-*d*<sub>6</sub>, 400 MHz):  $\delta$  ppm 1.93 (s, 9H), 4.10 (d, 2H,  $J$  = 6.0 Hz), 6.95 (d, 1H,  $J$  = 8.8 Hz), 7.23 (d, 2H,  $J$  = 8.3 Hz), 7.37 (t, 1H,  $J$  = 6.8 Hz), 7.57 (dd, 1H,  $J$  = 8.8, 2.6 Hz), 7.62 (d, 2H,  $J$  = 8.3 Hz), 8.08 (d, 1H,  $J$  = 2.6 Hz), 10.44 (s, 1H), 11.93 (bs, 1H); <sup>13</sup>C NMR (CDCl<sub>3</sub>, 100 MHz):  $\delta$  ppm 28.2, 43.0, 77.8, 110.0, 119.6, 119.9, 120.8, 127.3, 131.1, 135.8, 136.2, 136.5, 155.8, 157.6, 164.9; HPLC, RT = 2.00 min; MS (ESI<sup>+</sup>):  $m/z$  443.0 [M + Na]<sup>+</sup>, 445.0 [M + 2 + Na]<sup>+</sup>, 367.0 [M + H - *t*-Bu]<sup>+</sup>, 365.0 [M + H + 2 - *t*-Bu]<sup>+</sup>; HRMS calcd for C<sub>19</sub>H<sub>21</sub>BrN<sub>2</sub>NaO<sub>4</sub> 443.0577, found 443.0575.

**tert-Butyl (4-(5-Methoxy-2-hydroxybenzoyl))-aminobenzylcarbamate (10).** White solid ( $m$  = 75 mg, 45% yield); <sup>1</sup>H NMR (DMSO-*d*<sub>6</sub>, 300 MHz):  $\delta$  ppm 1.39 (s, 9H), 3.76 (s, 3H), 4.10 (d, 2H,  $J$  = 5.9 Hz), 6.92 (d, 1H,  $J$  = 8.9 Hz), 7.06 (ddd, 1H,  $J$  = 9.0, 9.0, 3.0 Hz), 7.23 (d, 2H,  $J$  = 8.3 Hz), 7.37 (bt, 1H,  $J$  = 5.9 Hz), 7.50 (d, 1H,  $J$  = 3.0 Hz), 7.62 (d, 2H,  $J$  = 8.3 Hz), 10.90 (s, 1H); <sup>13</sup>C NMR (DMSO-*d*<sub>6</sub>, 75 MHz):  $\delta$  ppm 28.2, 43.0, 55.7, 77.8, 112.5, 117.3, 118.1, 120.6, 121.0, 127.4, 136.1, 136.6, 151.8, 152.3, 155.8, 166.0; HPLC, RT = 1.78 min; MS (ESI<sup>+</sup>):  $m/z$  395.1 [M + Na]<sup>+</sup>, 373.1 [M + H]<sup>+</sup>; 317.1 [M + H - *t*-Bu]<sup>+</sup>.

**tert-Butyl (4-(4-Isopropyl-2-hydroxybenzoyl))-aminobenzylcarbamate (11).** Elution: *n*-Hex/AcOEt 3/1 v/v; white solid ( $m$  = 53 mg, 31% yield); <sup>1</sup>H NMR (CDCl<sub>3</sub>, 400 MHz):  $\delta$  ppm 1.60 (d, 6H,  $J$  = 6.7 Hz), 1.83 (s, 9H), 3.24 (hept, 1H,  $J$  = 6.7 Hz), 4.64 (d, 2H,  $J$  = 4.0 Hz), 5.25 (bs, 1H), 7.12 (d, 1H,  $J$  = 7.1 Hz), 7.60 (d, 2H,  $J$  = 7.6 Hz), 7.86 (m, 3H), 8.47 (bs, 1H), 12.30 (bs, 1H); <sup>13</sup>C NMR (CDCl<sub>3</sub>, 100 MHz):  $\delta$  ppm 23.7, 28.6, 34.4, 44.4, 79.9, 112.5, 116.5, 117.9, 121.7, 125.8, 128.3, 136.0, 136.2, 156.2, 156.9, 162.1, 168.6; HPLC, RT = 2.09 min; MS (ESI<sup>+</sup>):  $m/z$  407.1 [M + Na]<sup>+</sup>, 385.2 [M + H]<sup>+</sup>.

**tert-Butyl (4-(4-Trifluoromethyl-2-hydroxybenzoyl))-aminobenzylcarbamate (12).** Elution DCM/EtOH 99/1 v/v; white solid ( $m$  = 114 mg, 62% yield); mp: 179.5–180.5 °C; <sup>1</sup>H NMR (CD<sub>3</sub>OD, 400 MHz):  $\delta$  ppm 1.46 (s, 9H), 4.22 (s, 2H), 4.76 (bs, 1H), 7.22 (m, 2H), 7.29 (d, 2H,  $J$  = 8.4 Hz), 7.63 (d, 2H,  $J$  = 8.4 Hz), 8.11 (d, 1H,  $J$  = 8.6 Hz); <sup>13</sup>C NMR (CD<sub>3</sub>OD, 100 MHz):  $\delta$  ppm 28.8, 44.6, 80.2, 115.2 (d,  $J$  = 3.7 Hz), 116.5 (d,  $J$  = 3.7 Hz), 122.0, 122.5, 126.3, 128.7, 131.2, 135.8, 137.8, 158.6, 160.4, 165.2, 167.4; HPLC, RT = 1.86 min; MS (ESI<sup>+</sup>):  $m/z$  433.0 [M + Na]<sup>+</sup>, 411.1 [M + H]<sup>+</sup>, 355.0 [M + H - *t*-Bu]<sup>+</sup>; HRMS calcd for C<sub>20</sub>H<sub>22</sub>F<sub>3</sub>N<sub>2</sub>O<sub>4</sub> 411.1526, found 411.1537.

**tert-Butyl (4-(4-Fluoro-2-hydroxybenzoyl))-aminobenzylcarbamate (13).** Elution DCM/EtOH 99/1 v/v; white solid ( $m$  = 37 mg, 23% yield); mp: 155–5–156.5 °C; <sup>1</sup>H NMR (CD<sub>3</sub>OD, 400 MHz):  $\delta$  ppm 1.45 (s, 9H), 4.21 (s, 2H), 6.64–6.70 (m, 2H), 7.26 (d, 2H,  $J$  = 8.4 Hz), 7.59 (d, 2H,  $J$  = 8.4 Hz), 7.98 (dd, 1H,  $J$  = 9.4, 8.4 Hz); <sup>19</sup>F NMR (CD<sub>3</sub>OD, 400 MHz):  $\delta$  ppm -107.1; <sup>13</sup>C NMR (CD<sub>3</sub>OD, 100 MHz):  $\delta$  ppm 28.9, 44.8, 80.3, 105.2 (d,  $J$  = 24.2 Hz), 107.6 (d,  $J$  = 24.2 Hz), 114.8, 122.7, 128.8, 132.1 (d,  $J$  = 11.1 Hz), 132.5, 137.5, 138.0, 163.3 (d,  $J$  = 13.3 Hz), 167.4 (d,  $J$  = 251.3 Hz), 168.4; HPLC, RT = 1.88 min; MS (ESI<sup>+</sup>):  $m/z$  383.1 [M + Na]<sup>+</sup>, 361.1 [M + H]<sup>+</sup>, 305.1 [M + H - *t*-Bu]<sup>+</sup>; HRMS calcd for C<sub>19</sub>H<sub>22</sub>FN<sub>2</sub>O<sub>4</sub> 361.1558, found 361.1554.

**tert-Butyl (4-(1-Hydroxy-2-naphthoyl))aminobenzylcarbamate (14).** Elution: *n*-Hex/AcOEt 3/1 v/v; white solid ( $m$  = 40 mg, 23% yield); mp: 145–146 °C; <sup>1</sup>H NMR (DMSO-*d*<sub>6</sub>, 300 MHz):  $\delta$  ppm 1.40 (s, 9H), 4.13 (d, 2H,  $J$  = 5.9 Hz), 7.27 (d, 2H,  $J$  = 8.1 Hz), 7.40 (bt, 1H,  $J$  = 5.9 Hz), 7.46 (d, 1H,  $J$  = 8.9 Hz), 7.58 (dd, 1H,  $J$  = 8.1, 7.1 Hz), 7.68 (m, 3H), 7.92 (d, 1H,  $J$  = 8.1 Hz), 8.10 (d, 1H,  $J$  = 9.0 Hz), 8.31 (d, 1H,  $J$  = 8.1 Hz), 10.92 (bs, 1H); <sup>13</sup>C NMR (DMSO-*d*<sub>6</sub>, 75 MHz):  $\delta$  ppm 28.2, 43.0, 77.8, 107.5, 117.7, 121.1, 123.0, 124.7, 125.9, 127.2, 127.5, 129.1, 136.0, 136.1, 136.7, 155.8, 160.0, 169.4; HPLC, RT = 2.13 min; MS (ESI<sup>+</sup>):  $m/z$  415.1 [M + Na]<sup>+</sup>, 337.0 [M + H - *t*-Bu]<sup>+</sup>; HRMS calcd for C<sub>23</sub>H<sub>25</sub>N<sub>2</sub>O<sub>4</sub> 393.1809, found 393.1807.

**tert-Butyl (4-(2-Hydroxy-1-naphthoyl))aminobenzylcarbamate (15).** Elution: DCM/EtOH 98.5/1.5 v/v; white solid ( $m$  = 90 mg, 51% yield); mp: 188.5–189.5 °C; <sup>1</sup>H NMR (CDCl<sub>3</sub>, 300 MHz):  $\delta$  ppm 1.45 (s, 9H), 4.28 (d, 2H,  $J$  = 5.6 Hz), 4.88 (bs, 1H), 7.16 (d, 1H,  $J$  = 9.0 Hz), 7.29 (d, 2H,  $J$  = 8.8 Hz), 7.36 (dd, 1H,  $J$  = 7.4, 6.8 Hz), 7.54 (m, 3H), 7.81 (m, 2H), 8.01 (bs, 1H), 8.14 (d, 1H,  $J$  = 8.6 Hz), 10.92 (bs, 1H); <sup>13</sup>C NMR (CDCl<sub>3</sub>, 75 MHz):  $\delta$  ppm 28.6, 44.4, 79.9, 110.3, 119.5, 121.0, 122.6, 123.8, 128.4, 128.6, 129.0, 129.7, 130.7, 134.4, 136.2, 136.3, 156.0, 159.7, 168.5; HPLC, RT = 1.74 min; MS (ESI<sup>+</sup>):  $m/z$  415.1 [M + Na]<sup>+</sup>, 337.0 [M + H - *t*-Bu]<sup>+</sup>; HRMS calcd for C<sub>23</sub>H<sub>25</sub>N<sub>2</sub>O<sub>4</sub> 393.1809, found 393.1801.

**tert-Butyl (4-(3-Hydroxy-2-naphthoyl))aminobenzylcarbamate (16).** White solid ( $m$  = 56 mg, 32% yield); mp: 199–200 °C; <sup>1</sup>H NMR (DMSO-*d*<sub>6</sub>, 400 MHz):  $\delta$  ppm 1.40 (s, 9H), 4.11 (d, 2H,  $J$  = 6.1 Hz), 7.25 (d, 2H,  $J$  = 8.4 Hz), 7.32 (s, 1H), 7.35 (m, 2H), 7.50 (ddd, 1H,  $J$  = 8.4, 6.8, 1.0 Hz), 7.69 (d, 2H,  $J$  = 8.4 Hz), 7.75 (d, 1H,  $J$  = 8.2 Hz), 7.92 (d, 1H,  $J$  = 8.2 Hz), 8.51 (s, 1H), 10.65 (bs, 1H); <sup>13</sup>C NMR (DMSO-*d*<sub>6</sub>, 100 MHz):  $\delta$  ppm 28.2, 43.0, 77.7, 110.6, 120.5, 121.6, 123.7, 125.7, 126.8, 127.4, 128.1, 128.7, 130.4, 135.8, 135.9, 137.0, 154.0, 155.8, 165.6; HPLC, RT = 1.99 min; MS (ESI<sup>+</sup>):  $m/z$  415.2 [M + Na]<sup>+</sup>, 337.1 [M + H - *t*-Bu]<sup>+</sup>; HRMS calcd for C<sub>23</sub>H<sub>25</sub>N<sub>2</sub>O<sub>4</sub> 393.1809, found 393.1810.

**tert-Butyl (4-(2-Naphthoyl))aminobenzylcarbamate (17).** White solid ( $m$  = 61 mg, 36% yield); mp: 182.5–183.5 °C; <sup>1</sup>H NMR (CDCl<sub>3</sub>, 400 MHz):  $\delta$  ppm 1.45 (s, 9H), 4.28 (d, 2H,  $J$  = 5.3 Hz), 4.86 (bs, 1H), 7.28 (d, 2H,  $J$  = 8.4 Hz), 7.56 (m, 2H), 7.63 (d, 2H,  $J$  = 8.4 Hz), 7.91 (m, 4H), 8.03 (bs, 1H), 8.36 (s, 1H); <sup>13</sup>C NMR (CDCl<sub>3</sub>, 100 MHz):  $\delta$  ppm 28.6, 44.5, 79.8, 120.7, 123.8, 127.2, 127.8, 128.0, 128.1, 128.5, 129.0, 129.2, 132.3, 132.8, 135.1, 135.4, 137.4, 156.1, 166.0; HPLC, RT = 1.91 min; MS (ESI<sup>+</sup>):  $m/z$  377.1 [M + H]<sup>+</sup>, 399.1 [M + Na]<sup>+</sup>, 321.3 [M + H - *t*-Bu]<sup>+</sup>; HRMS calcd for C<sub>23</sub>H<sub>25</sub>N<sub>2</sub>O<sub>3</sub> 377.1860, found 377.1855.

**tert-Butyl (1*H*-2-Indolylcarbonyl)aminobenzylcarbamate (18).** White solid ( $m$  = 67 mg, 41% yield); mp: 207–208 °C; <sup>1</sup>H NMR (DMSO-*d*<sub>6</sub>, 400 MHz):  $\delta$  ppm 1.40 (s, 9H), 4.10 (s, 2H), 7.06 (t, 1H,  $J$  = 7.5 Hz), 7.22 (m, 3H), 7.36 (bs, 1H), 7.40 (s, 1H), 7.46 (d, 1H,  $J$  = 8.3 Hz), 7.66 (d, 1H,  $J$  = 7.5 Hz), 7.72 (d, 2H,  $J$  = 8.3 Hz), 10.2 (bs, 1H), 11.76 (bs, 1H); <sup>13</sup>C NMR (DMSO-*d*<sub>6</sub>, 100 MHz):  $\delta$  ppm 28.3, 40.0, 77.7, 103.8, 112.4, 119.8, 120.1, 121.7, 123.7, 127.0, 127.3, 131.6, 135.3, 136.9, 137.5, 155.7, 159.7; HPLC, RT = 1.82 min; MS (ESI<sup>+</sup>):  $m/z$  388.2 [M + Na]<sup>+</sup>, 310.2 [M + H - *t*-Bu]<sup>+</sup>; HRMS calcd for C<sub>21</sub>H<sub>24</sub>N<sub>3</sub>O<sub>3</sub> 366.1812, found 366.1812.

**tert-Butyl 4-[(4-Oxo-1,4-dihydroquinolin-3-yl)carbonyl]aminobenzylcarbamate (19).** White solid ( $m$  = 48 mg, 27% yield); mp: 238–239 °C; <sup>1</sup>H NMR (DMSO-*d*<sub>6</sub>, 400 MHz):  $\delta$  ppm 1.40 (s, 9H), 4.08 (d, 2H,  $J$  = 6.0 Hz), 7.17 (d, 2H,  $J$  = 8.3 Hz), 7.24 (td, 1H,  $J$  = 8.1, 1.1 Hz), 7.33 (t, 1H,  $J$  = 6.1 Hz), 7.50 (td, 1H,  $J$  = 8.1, 1.5 Hz), 7.59 (d, 1H,  $J$  = 8.1 Hz), 7.66 (d, 2H,  $J$  = 8.3 Hz), 8.24 (dd, 1H,  $J$  = 8.1, 1.1 Hz), 8.87 (s, 1H), 13.64 (s, 1H); <sup>13</sup>C NMR (DMSO-*d*<sub>6</sub>, 100 MHz):  $\delta$  ppm 28.3, 43.1, 77.7, 108.6, 118.9, 122.2, 124.7, 126.7, 127.5, 127.6, 129.3, 133.5, 139.0, 149.3, 151.6, 155.8, 166.1, 174.0; HPLC, RT = 1.67 min; MS (ESI<sup>+</sup>):  $m/z$  394.2 [M + H]<sup>+</sup>, 338.2 [M + H - *t*-Bu]<sup>+</sup>; HRMS calcd for C<sub>22</sub>H<sub>24</sub>N<sub>3</sub>O<sub>4</sub> 394.1761, found 394.1756.

**tert-Butyl (4-(3-Hydroxypyridin-2-yl))aminobenzylcarbamate (20).** Light yellow solid ( $m$  = 30 mg, 19% yield); mp: 90–92 °C; <sup>1</sup>H NMR (CDCl<sub>3</sub>, 400 MHz):  $\delta$  ppm 1.45 (s, 9H), 4.29 (d, 2H,  $J$  = 5.7 Hz), 7.30 (d, 2H,  $J$  = 8.4 Hz), 7.31–7.37 (m, 2H), 7.65 (d, 2H,  $J$

= 8.4 Hz), 8.06 (bs, 1H), 8.10 (dd, 1H,  $J = 4.1, 1.6$  Hz), 9.90 (bs, 1H), 11.89 (s, 1H); HPLC, RT = 1.85 min; MS (ESI+):  $m/z$  366.1 [M + Na]<sup>+</sup>.

**tert-Butyl (4-(6-Methoxy-1-hydroxy-2-naphthoyl))-aminobenzylcarbamate (21).** White solid ( $m = 34$  mg, 18% yield); mp: 205.8–206.3 °C; <sup>1</sup>H NMR (CDCl<sub>3</sub>, 300 MHz):  $\delta$  ppm 1.48 (s, 9H), 3.94 (s, 3H), 4.30 (d, 2H,  $J = 5.4$  Hz), 4.87 (bs, 1H), 7.07 (d, 1H,  $J = 2.3$  Hz), 7.16 (dd, 1H,  $J = 9.1, 2.4$  Hz), 7.20 (d, 1H,  $J = 8.1$  Hz), 7.30 (d, 2H,  $J = 8.3$  Hz), 7.44 (d, 1H,  $J = 9.1$  Hz), 7.55 (d, 2H,  $J = 8.3$  Hz), 7.98 (bs, 1H), 8.35 (d, 1H,  $J = 9.1$  Hz); <sup>13</sup>C NMR (CDCl<sub>3</sub>, 75 MHz):  $\delta$  ppm 28.6, 44.4, 55.5, 79.3, 105.4, 106.2, 117.6, 118.2, 121.0, 121.6, 121.7, 125.9, 128.4, 136.0, 136.2, 138.6, 142.7, 143.1, 160.6, 161.6; HPLC, RT = 2.14 min; MS (ESI+):  $m/z$  445.2 [M + Na]<sup>+</sup>, 367.1 [M + H - t-Bu]<sup>+</sup>; HRMS calcd for C<sub>24</sub>H<sub>27</sub>N<sub>2</sub>O<sub>5</sub> 423.1914, found 423.1911.

**tert-Butyl (4-(7-Methoxy-1-hydroxy-2-naphthoyl))-aminobenzylcarbamate (22).** White solid ( $m = 30$  mg, 16% yield); <sup>1</sup>H NMR (CDCl<sub>3</sub>, 400 MHz):  $\delta$  ppm 1.40 (s, 9H), 3.89 (s, 3H), 4.24 (d, 2H,  $J = 5.4$  Hz), 4.81 (bs, 1H), 7.17–7.29 (m, 6H), 7.49 (d, 1H,  $J = 8.3$  Hz), 7.60 (d, 1H,  $J = 8.9$  Hz), 7.65 (d, 1H,  $J = 2.4$  Hz), 7.98 (bs, 1H), 13.38 (s, 1H); <sup>13</sup>C NMR (CDCl<sub>3</sub>, 400 MHz):  $\delta$  ppm 28.6, 29.9, 44.4, 55.7, 79.9, 102.2, 107.4, 118.5, 118.6, 121.7, 122.0, 126.9, 128.5, 129.1, 131.9, 136.2, 156.1, 158.3, 160.3, 169.5; HPLC, RT = 2.12 min; MS (ESI+):  $m/z$  423.1 [M + H]<sup>+</sup>,  $m/z$  845.3 [2M + H]<sup>+</sup>,  $m/z$  440.2 [M + NH<sub>4</sub>]<sup>+</sup>.

**tert-Butyl (4-(7-Methyl-1-hydroxy-2-naphthoyl))-aminobenzylcarbamate (23).** Elution: *n*-Hex/AcOEt 4/1 v/v; white solid ( $m = 140$  mg, 77% yield); mp: 188.3–188.9 °C; <sup>1</sup>H NMR (CDCl<sub>3</sub>, 500 MHz):  $\delta$  ppm 1.41 (s, 9H), 2.47 (s, 3H), 4.22 (d, 2H,  $J = 5.8$  Hz), 4.84 (bt, 1H), 7.20 (m, 3H), 7.34 (d, 1H,  $J = 9.0$  Hz), 7.36 (dd, 1H,  $J = 8.4, 1.4$  Hz), 7.46 (d, 1H,  $J = 8.1$  Hz), 7.60 (d, 1H,  $J = 8.4$  Hz), 8.05 (bs, 1H), 8.15 (s, 1H), 13.45 (s, 1H); <sup>13</sup>C NMR (CDCl<sub>3</sub>, 125 MHz):  $\delta$  ppm 22.0, 28.6, 44.3, 79.9, 107.0, 118.5, 120.0, 121.8, 123.0, 125.9, 127.4, 128.4, 131.6, 134.8, 136.0, 136.1, 136.2, 156.1, 161.0, 169.5; HPLC, RT = 2.23 min; MS (ESI+):  $m/z$  429.1 [M + Na]<sup>+</sup>, 407.2 [M + H]<sup>+</sup>, 351.1 [M + H - t-Bu]<sup>+</sup>; HRMS calcd for C<sub>24</sub>H<sub>27</sub>N<sub>2</sub>O<sub>4</sub> 407.1965, found 407.1962.

**tert-Butyl (4-(7-Chloro-1-hydroxy-2-naphthoyl))-aminobenzylcarbamate (24).** White solid ( $m = 101$  mg, 53% yield); <sup>1</sup>H NMR (CDCl<sub>3</sub>, 400 MHz):  $\delta$  ppm 1.58 (s, 9H), 4.32 (d, 2H,  $J = 5.7$  Hz), 4.88 (bs, 1H), 7.33 (m, 3H), 7.48 (d, 1H,  $J = 8.8$  Hz), 7.55 (dd, 1H,  $J = 8.8, 2.2$  Hz), 7.57 (d, 2H,  $J = 8.3$  Hz), 7.72 (d, 1H,  $J = 8.7$  Hz), 8.00 (s, 1H), 8.43 (d, 1H,  $J = 2.2$  Hz), 13.51 (s, 1H); <sup>13</sup>C NMR (CDCl<sub>3</sub>, 400 MHz):  $\delta$  ppm 28.6, 44.4, 79.9, 107.7, 118.4, 121.1, 121.7, 123.4, 126.6, 128.5, 129.2, 130.2, 132.4, 134.7, 135.9, 136.4, 156.1, 160.6, 169.0; HPLC, RT = 2.12 min; MS (ESI+):  $m/z$  371.1 [M + H - t-Bu]<sup>+</sup>, 373.1 [M + H - t-Bu + 2]<sup>+</sup>, 444.1 [M + NH<sub>4</sub>]<sup>+</sup>, 446.1 [M + NH<sub>4</sub> + 2]<sup>+</sup>, 427.1 [M + H]<sup>+</sup>, 429.1 [M + H + 2]<sup>+</sup>.

**tert-Butyl (4-(6,7-Dimethoxy-1-hydroxy-2-naphthoyl))-aminobenzylcarbamate (25).** Elution: *n*-Hex/AcOEt 2/1 v/v; white solid ( $m = 140$  mg, 69% yield); <sup>1</sup>H NMR (CDCl<sub>3</sub>, 400 MHz):  $\delta$  ppm 1.47 (s, 9H), 4.02 (s, 3H), 4.04 (s, 3H), 4.31 (d, 2H,  $J = 5.4$  Hz), 4.87 (bs, 1H), 7.07 (s, 1H), 7.18 (d, 1H,  $J = 8.7$  Hz), 7.30 (d, 2H,  $J = 8.3$  Hz), 7.36 (d, 1H,  $J = 8.8$  Hz), 7.56 (d, 2H,  $J = 8.3$  Hz), 7.70 (s, 1H), 8.01 (s, 1H), 13.44 (s, 1H); <sup>13</sup>C NMR (CDCl<sub>3</sub>, 100 MHz):  $\delta$  ppm 28.6, 44.4, 56.2, 56.3, 79.8, 102.9, 106.1, 106.5, 117.3, 119.5, 120.7, 121.7, 128.5, 131.1, 133.0, 136.0, 136.3, 149.6, 152.1, 160.2, 169.5; HPLC, RT = 3.81 min; MS (ESI+):  $m/z$  397.2 [M + H - t-Bu]<sup>+</sup>, 453.3 [M + H]<sup>+</sup>, 475.3 [M + Na]<sup>+</sup>.

**Synthesis of tert-Butyl (4-(5-tert-Butyl-2-hydroxybenzyl)amino)benzylcarbamate (29).** To a solution of 100 mg of compound 2 (0.45 mmol) in 2.5 mL of ethanol was added 80 mg of aldehyde 26 (0.45 mmol, 1 equiv). The solution was stirred at reflux for 6 h. After cooling to room temperature, 9 mg of sodium borohydride (0.235 mmol, 0.5 equiv) was added and the solution was stirred at room temperature for 1 h 30 min. Then, 20 mL of water was added and the solution was extracted with ethyl acetate (3 × 20 mL). The organic layer was dried over Na<sub>2</sub>SO<sub>4</sub>, filtered, and the solvent was evaporated *in vacuo* to offer compound 30 as a white solid ( $m = 110$  mg, 64% yield); mp 102.0–103.0 °C; <sup>1</sup>H NMR (CDCl<sub>3</sub>, 300 MHz):  $\delta$  ppm

1.29 (s, 9H), 1.44 (s, 9H), 4.19 (d, 2H,  $J = 5.6$  Hz), 4.35 (s, 2H), 4.81 (bs, 2H), 6.76 (d, 2H,  $J = 8.4$  Hz), 6.81 (d, 1H), 7.12 (m, 3H), 7.21 (dd, 1H,  $J = 8.4, 2.4$  Hz), 11.2 (s, 1H); <sup>13</sup>C NMR (CDCl<sub>3</sub>, 75 MHz):  $\delta$  ppm 28.6, 31.7, 44.4, 48.8, 64.9, 79.6, 115.8, 116.1, 122.4, 124.9, 125.8, 126.1, 128.8, 130.9, 143.0, 146.9, 154.2; HPLC, RT = 3.57 min; MS (ESI+):  $m/z$  329.1 [M + H - t-Bu]<sup>+</sup>, 385.1 [M + H]<sup>+</sup>, 407.1 [M + Na]<sup>+</sup>; HRMS calcd for C<sub>23</sub>H<sub>33</sub>N<sub>2</sub>O<sub>3</sub> 385.2486, found 385.2499.

**Synthesis of tert-Butyl 4-[(1-Hydroxy-2-naphthoyl)amino]piperidine-1-carboxylate (52).** To a solution of 91 mg of compound 1-Boc-4-aminopiperidine (0.45 mmol) in 2.5 mL of THF were added 86 mg of 1-hydroxy-2-naphthoic acid (1 equiv, 0.45 mmol) and 103 mg of EDCI (1 equiv, 0.45 mmol). The solution was stirred at reflux for 12 h. After cooling to room temperature, the solution was evaporated to dryness. The crude product was dissolved in 20 mL of ethyl acetate, and the solution was washed with 1 N hydrochloric acid solution (3 × 20 mL) and then by 10% aqueous sodium carbonate solution. The organic layer was dried over Na<sub>2</sub>SO<sub>4</sub>, filtered, and the solvent was evaporated *in vacuo*. The resulting crude mixture was purified by chromatography on silica gel and eluted by *n*-Hex/AcOEt 3/1 v/v to offer compound 52 as a white solid ( $m = 38$  mg, 23% yield); <sup>1</sup>H NMR (CDCl<sub>3</sub>, 400 MHz):  $\delta$  ppm 1.23 (m, 1H), 1.42 (m, 1H), 1.46 (s, 9H), 2.04 (m, 2H), 2.90 (t, 2H,  $J = 12.1$  Hz), 4.07–4.19 (m, 3H), 6.25 (d, 1H,  $J = 7.7$  Hz), 7.23 (d, 1H,  $J = 8.8$  Hz), 7.28 (d, 1H,  $J = 8.9$  Hz), 7.50 (td, 1H,  $J = 8.2, 1.3$  Hz), 7.56 (td, 1H,  $J = 8.2, 1.3$  Hz), 7.74 (d, 1H,  $J = 7.8$  Hz), 8.40 (d, 1H,  $J = 8.2$  Hz), 13.75 (s, 1H); <sup>13</sup>C NMR (CDCl<sub>3</sub>, 100 MHz):  $\delta$  ppm 28.6, 29.8, 32.2, 47.3, 80.0, 106.6, 118.3, 120.9, 124.0, 125.8, 126.0, 127.4, 129.1, 136.4, 154.8, 160.9, 170.2; HPLC, RT = 2.16 min; MS (ESI+):  $m/z$  371.2 [M + H]<sup>+</sup>, 315.2 [M + H - t-Bu]<sup>+</sup>.

**General Procedure for the Synthesis of Compounds 28–51 and 53.** Compound 3–25, 27, or 52 (0.2 mmol) in 5 mL of 6 N HCl in dioxane was stirred at room temperature for 1 h 30 min. The dioxane was evaporated, and the crude product was washed with diethyl ether to offer a deprotected compound as a hydrochloride salt.

***N*-(4-(Aminomethyl)phenyl)-5-tert-butyl-2-hydroxybenzamide Hydrochloride (28).** White solid ( $m = 54$  mg, 80% yield); mp: 268–269 °C; <sup>1</sup>H NMR (DMSO-*d*<sub>6</sub>, 300 MHz):  $\delta$  ppm 1.30 (s, 9H), 3.56 (s, 1H), 3.99 (s, 2H), 6.97 (d, 1H,  $J = 8.2$  Hz), 7.50 (m, 3H), 7.72 (d, 2H,  $J = 7.0$  Hz), 7.94 (s, 1H), 8.42 (bs, 3H), 10.52 (s, 1H); <sup>13</sup>C NMR (DMSO-*d*<sub>6</sub>, 75 MHz):  $\delta$  ppm 31.2, 41.8, 66.3, 116.7, 116.9, 120.9, 122.8, 125.5, 129.4, 130.6, 138.3, 141.3, 155.7, 166.3; HPLC, RT = 1.45 min; HRMS calcd for C<sub>18</sub>H<sub>23</sub>N<sub>2</sub>O<sub>2</sub> 299.1754, found 299.1752.

**2-(4-(Aminomethyl)phenyl)aminomethyl)-4-tert-butylphenol Hydrochloride (29).** White solid ( $m = 52$  mg, 73% yield); mp: 258–260 °C (dec.); <sup>1</sup>H NMR (DMSO-*d*<sub>6</sub>, 300 MHz):  $\delta$  ppm 1.20 (s, 9H), 3.93 (d, 2H,  $J = 5.2$  Hz), 4.31 (bs, 2H), 6.81 (d, 1H,  $J = 8.4$  Hz), 7.15 (m, 3H), 7.42 (m, 3H), 8.45 (bs, 3H), 10.43 (s, 1H); <sup>13</sup>C NMR (DMSO-*d*<sub>6</sub>, 75 MHz):  $\delta$  ppm 31.4, 33.7, 41.7, 46.3, 114.7, 119.0, 120.0, 123.2, 125.8, 127.5, 130.0, 130.3, 140.9, 153.3; HPLC, RT = 1.39 min; HRMS calcd for C<sub>18</sub>H<sub>25</sub>N<sub>2</sub>O 285.1961, found 285.1954.

***N*-(4-(Aminomethyl)phenyl)-2-hydroxybenzamide Hydrochloride (30).** White solid ( $m = 45$  mg, 81% yield); mp: 275–276 °C (dec.); <sup>1</sup>H NMR (DMSO-*d*<sub>6</sub>, 300 MHz):  $\delta$  ppm 3.99 (d, 2H,  $J = 4.9$  Hz), 6.96 (t, 1H,  $J = 7.5$  Hz), 7.04 (d, 1H,  $J = 8.4$  Hz), 7.43 (dd, 1H,  $J = 8.4, 7.2$  Hz), 7.49 (d, 2H,  $J = 8.4$  Hz), 7.75 (d, 2H,  $J = 8.4$  Hz), 8.01 (d, 1H,  $J = 7.2$  Hz), 8.45 (bs, 3H), 10.51 (s, 1H); <sup>13</sup>C NMR (DMSO-*d*<sub>6</sub>, 75 MHz):  $\delta$  ppm 41.7, 117.2, 117.5, 119.0, 120.8, 129.2, 129.4, 129.5, 133.6, 138.3, 158.2, 166.4; HPLC, RT = 1.05 min; MS (ESI+):  $m/z$  244.1 [M + H + 1]<sup>+</sup>; HRMS calcd for C<sub>14</sub>H<sub>15</sub>N<sub>2</sub>O<sub>2</sub> 243.1128, found 243.1129.

***N*-(4-(Aminomethyl)phenyl)-3-methyl-2-hydroxybenzamide Hydrochloride (31).** Beige solid ( $m = 54$  mg, 92% yield); mp: 275–276 °C; <sup>1</sup>H NMR (DMSO-*d*<sub>6</sub>, 400 MHz):  $\delta$  ppm 2.20 (s, 3H), 4.00 (q, 2H,  $J = 5.6$  Hz), 6.88 (t, 1H,  $J = 7.7$  Hz), 7.38 (d, 1H,  $J = 7.7$  Hz), 7.51 (d, 2H,  $J = 8.4$  Hz), 7.75 (d, 2H,  $J = 8.4$  Hz), 8.00 (d, 1H,  $J = 7.7$  Hz), 8.45 (bs, 3H), 10.59 (s, 1H), 12.53 (s, 1H); <sup>13</sup>C NMR (DMSO-*d*<sub>6</sub>, 100 MHz):  $\delta$  ppm 15.5, 41.7, 114.1, 118.0, 121.9, 125.5, 126.1, 129.4, 130.1, 135.1, 137.8, 159.2, 169.2; HPLC, RT = 1.22 min; HRMS calcd for C<sub>15</sub>H<sub>17</sub>N<sub>2</sub>O<sub>2</sub> 257.1285, found 257.1292.



*N*-(4-(Aminomethyl)phenyl)-4-methyl-2-hydroxybenzamide Hydrochloride (**32**). Beige solid (*m* = 53 mg, 90% yield); mp: 282–283 °C (dec.); <sup>1</sup>H NMR (DMSO-*d*<sub>6</sub>, 400 MHz): δ ppm 2.30 (s, 3H), 3.98 (q, 2H, *J* = 5.6 Hz), 6.78 (d, 1H, *J* = 8.2 Hz), 6.84 (s, 1H), 7.48 (d, 2H, *J* = 8.4 Hz), 7.74 (d, 2H, *J* = 8.4 Hz), 7.94 (d, 1H, *J* = 8.2 Hz), 8.43 (bs, 3H), 10.46 (s, 1H); <sup>13</sup>C NMR (DMSO-*d*<sub>6</sub>, 100 MHz): δ ppm 21.1, 41.8, 114.2, 117.5, 120.1, 120.9, 129.0, 129.5, 130.3, 138.3, 144.4, 158.8, 166.7; HPLC, RT = 1.11 min; HRMS calcd for C<sub>15</sub>H<sub>17</sub>N<sub>2</sub>O<sub>2</sub> 257.1285, found 257.1293.

*N*-(4-(Aminomethyl)phenyl)-5-methyl-2-hydroxybenzamide Hydrochloride (**33**). White solid (*m* = 58 mg, 99% yield); mp: 292–293 °C (dec.); <sup>1</sup>H NMR (DMSO-*d*<sub>6</sub>, 400 MHz): δ ppm 2.28 (s, 3H), 3.98 (q, 2H, *J* = 5.4 Hz), 6.92 (d, 1H, *J* = 8.3 Hz), 7.24 (d, 1H, *J* = 8.3 Hz), 7.48 (d, 2H, *J* = 8.4 Hz), 7.74 (d, 2H, *J* = 8.4 Hz), 7.82 (s, 1H), 8.42 (bs, 3H), 10.49 (s, 1H), 11.61 (s, 1H); <sup>13</sup>C NMR (DMSO-*d*<sub>6</sub>, 100 MHz): δ ppm 20.0, 41.8, 117.1, 120.7, 127.7, 129.1, 129.5, 130.2, 134.3, 138.4, 156.1, 166.5; HPLC, RT = 1.13 min; HRMS calcd for C<sub>15</sub>H<sub>17</sub>N<sub>2</sub>O<sub>2</sub> 257.1285, found 257.1289.

*N*-(4-(Aminomethyl)phenyl)-6-methyl-2-hydroxybenzamide Hydrochloride (**34**). White solid (*m* = 58 mg, 99% yield); mp: 251–252 °C (dec.); <sup>1</sup>H NMR (CD<sub>3</sub>OD, 300 MHz): δ ppm 2.32 (s, 3H), 4.10 (s, 2H), 6.72 (d, 1H, *J* = 8.0 Hz), 6.74 (d, 1H, *J* = 8.0 Hz), 7.13 (t, 1H, *J* = 8.0 Hz), 7.44 (d, 2H, *J* = 8.5 Hz), 7.78 (d, 2H, *J* = 8.5 Hz); <sup>13</sup>C NMR (DMSO-*d*<sub>6</sub>, 100 MHz): δ ppm 19.2, 44.0, 114.0, 121.7, 122.1, 126.6, 129.9, 130.6, 131.1, 137.5, 141.0, 155.5, 170.1; HPLC, RT = 0.88 min; HRMS calcd for C<sub>15</sub>H<sub>17</sub>N<sub>2</sub>O<sub>2</sub> 257.1285, found 257.1287.

*N*-(4-(Aminomethyl)phenyl)-5-bromo-2-hydroxybenzamide Hydrochloride (**35**). Yellow solid (*m* = 71 mg, 99% yield); mp: 309–310 °C; <sup>1</sup>H NMR (DMSO-*d*<sub>6</sub>, 400 MHz): δ ppm 4.00 (s, 2H), 7.01 (d, 1H, *J* = 8.8 Hz), 7.47 (d, 2H, *J* = 8.6 Hz), 7.58 (dd, 1H, *J* = 8.8, 2.4 Hz), 7.73 (d, 2H, *J* = 8.6 Hz), 8.07 (d, 1H, *J* = 2.4 Hz), 8.32 (bs, 3H), 10.50 (s, 1H), 11.90 (bs, 1H); <sup>13</sup>C NMR (CDCl<sub>3</sub>, 100 MHz): δ ppm 41.8, 110.2, 119.5, 120.7, 129.5, 129.7, 131.4, 135.9, 138.2, 157.1, 164.8; HPLC, RT = 1.21 min; HRMS calcd for C<sub>14</sub>H<sub>14</sub>N<sub>2</sub>O<sub>2</sub>Br 321.0233, found 321.0236.

*N*-(4-(Aminomethyl)phenyl)-5-methoxy-2-hydroxybenzamide Hydrochloride (**36**). White solid (*m* = 55 mg, 90% yield); mp: 277.5–278.5 °C; <sup>1</sup>H NMR (DMSO-*d*<sub>6</sub>, 300 MHz): δ ppm 3.76 (s, 3H), 4.00 (s, 2H), 6.95 (d, 1H, *J* = 8.8 Hz), 7.06 (dd, 1H, *J* = 8.8, 2.2 Hz), 7.47 (d, 2H, *J* = 8.1 Hz), 7.50 (d, 1H, *J* = 2.2 Hz), 7.74 (d, 2H, *J* = 8.1 Hz), 8.22 (bs, 3H), 10.54 (s, 1H); <sup>13</sup>C NMR (DMSO-*d*<sub>6</sub>, 75 MHz): δ ppm 41.8, 55.7, 112.7, 117.5, 118.2, 120.6, 120.8, 129.5, 129.6, 138.3, 151.8, 152.0, 165.9; HPLC, RT = 1.10 min; HRMS calcd for C<sub>15</sub>H<sub>17</sub>N<sub>2</sub>O<sub>3</sub> 273.1234, found 273.1240.

*N*-(4-(Aminomethyl)phenyl)-4-isopropyl-2-hydroxybenzamide Hydrochloride (**37**). White solid (*m* = 63 mg, 56% yield); mp: 282–283 °C; <sup>1</sup>H NMR (DMSO-*d*<sub>6</sub>, 400 MHz): δ ppm 1.20 (d, 6H, *J* = 6.8 Hz), 2.87 (hept, 1H, *J* = 6.8 Hz), 3.99 (d, 2H, *J* = 3.9 Hz), 6.87 (m, 2H), 7.48 (d, 2H, *J* = 8.3 Hz), 7.74 (d, 2H, *J* = 8.3 Hz), 7.95 (d, 1H, *J* = 7.9 Hz), 8.39 (bs, 3H), 10.5 (s, 1H), 11.97 (bs, 1H); <sup>13</sup>C NMR (DMSO-*d*<sub>6</sub>, 100 MHz): δ ppm 23.3, 33.3, 41.8, 114.6, 114.7, 117.4, 120.8, 129.0, 129.4, 138.3, 155.0, 158.8, 166.7; HPLC, RT = 1.33 min; HRMS calcd for C<sub>17</sub>H<sub>21</sub>N<sub>2</sub>O<sub>2</sub> 285.1598, found 285.1603.

*N*-(4-(Aminomethyl)phenyl)-4-trifluoromethyl-2-hydroxybenzamide Hydrochloride (**38**). White solid (*m* = 67 mg, 96% yield); mp: 270–272 °C (dec.); <sup>1</sup>H NMR (DMSO-*d*<sub>6</sub>, 400 MHz): δ ppm 3.99 (bs, 2H), 7.28 (d, 1H, *J* = 7.9 Hz), 7.39 (s, 1H), 7.48 (d, 2H, *J* = 8.1 Hz), 7.76 (d, 2H, *J* = 8.1 Hz), 8.03 (d, 1H, *J* = 7.9 Hz), 8.38 (bs, 3H), 10.54 (s, 1H), 11.97 (bs, 1H); <sup>19</sup>F (DMSO-*d*<sub>6</sub>, 400 MHz): –61.77; <sup>13</sup>C NMR (DMSO-*d*<sub>6</sub>, 100 MHz): δ ppm 41.8, 113.4, 115.3, 120.3, 122.1, 123.5, 129.5, 130.7, 132.3, 132.6, 138.4, 157.1, 164.5; HPLC, RT = 1.29 min; MS (ESI+): *m/z* 312.1 [M + H]<sup>+</sup>, 294.1 [M + H – NH<sub>3</sub>]<sup>+</sup>; HRMS calcd for C<sub>15</sub>H<sub>14</sub>F<sub>3</sub>N<sub>2</sub>O<sub>2</sub> 311.1002, found 311.1005.

*N*-(4-(Aminomethyl)phenyl)-4-fluoro-2-hydroxybenzamide Hydrochloride (**39**). White solid (*m* = 45 mg, 76% yield); mp: 280–281 °C; <sup>1</sup>H NMR (DMSO-*d*<sub>6</sub>, 400 MHz): δ ppm 3.99 (s, 2H), 6.88–6.80 (m, 2H), 7.48 (d, 2H, *J* = 8.4 Hz), 7.74 (d, 2H, *J* = 8.4 Hz), 8.08 (dd, 1H, *J* = 8.7, 8.7 Hz), 8.36 (bs, 3H), 10.47 (s, 1H), 12.36 (bs, 1H); <sup>19</sup>F NMR (DMSO-*d*<sub>6</sub>, 400 MHz): –105.70; <sup>13</sup>C NMR (DMSO-

*d*<sub>6</sub>, 100 MHz): δ ppm 41.8, 103.8 (d, *J* = 24.2 Hz), 106.5 (d, *J* = 24.2 Hz), 114.5, 120.9, 129.4, 129.6, 131.5 (d, *J* = 11 Hz), 138.2, 160.4 (d, *J* = 13.2 Hz), 164.8 (d, *J* = 249 Hz), 165.7; HPLC, RT = 1.09 min; HRMS calcd for C<sub>14</sub>H<sub>14</sub>N<sub>2</sub>O<sub>2</sub> 261.1034, found 261.1034.

*N*-(4-(Aminomethyl)phenyl)-1-hydroxy-2-naphthamide Hydrochloride (**40**). White solid (*m* = 63 mg, 99% yield); mp: 277–278 °C (dec.); <sup>1</sup>H NMR (DMSO-*d*<sub>6</sub>, 300 MHz): δ ppm 4.02 (s, 2H), 7.46 (d, 1H, *J* = 8.9 Hz), 7.53 (d, 2H, *J* = 8.3 Hz), 7.59 (d, 1H, *J* = 7.5 Hz), 7.68 (t, 1H, *J* = 7.5 Hz), 7.80 (d, 2H, *J* = 8.3 Hz), 7.92 (d, 1H, *J* = 8.0 Hz), 8.22 (d, 1H, *J* = 8.9 Hz), 8.31 (d, 1H, *J* = 8.3 Hz), 8.48 (bs, 3H), 10.43 (s, 1H); <sup>13</sup>C NMR (DMSO-*d*<sub>6</sub>, 75 MHz): δ ppm 41.8, 107.5, 117.8, 122.1, 123.1, 123.2, 124.6, 125.9, 127.5, 129.2, 129.4, 130.2, 136.0, 137.8, 160.0, 169.6; HPLC, RT = 1.45 min; MS (ESI+): *m/z* 294.1 [M + H + 1]<sup>+</sup>; HRMS calcd for C<sub>18</sub>H<sub>17</sub>N<sub>2</sub>O<sub>2</sub> 293.1290, found 293.1289.

*N*-(4-(Aminomethyl)phenyl)-2-hydroxy-1-naphthamide Hydrochloride (**41**). White powder (*m* = 57 mg, 97% yield); mp: 248–249 °C; <sup>1</sup>H NMR (DMSO-*d*<sub>6</sub>, 300 MHz): δ ppm 3.98 (d, 2H, *J* = 5.3 Hz), 7.32 (m, 2H), 7.45 (m, 3H), 7.67 (d, 1H, *J* = 8.3 Hz), 7.84 (m, 4H), 8.42 (bs, 3H), 10.22 (bs, 1H), 10.43 (s, 1H); <sup>13</sup>C NMR (DMSO-*d*<sub>6</sub>, 75 MHz): δ ppm 41.9, 118.4, 119.1, 122.9, 123.2, 126.9, 127.3, 127.9, 128.6, 129.5, 130.1, 131.3, 139.7, 151.7, 165.8; HPLC, RT = 1.11 min; MS (ESI+): *m/z* 294.1 [M + H + 1]<sup>+</sup>; HRMS calcd for C<sub>18</sub>H<sub>17</sub>N<sub>2</sub>O<sub>2</sub> 293.1285, found 293.1293.

*N*-(4-(Aminomethyl)phenyl)-3-hydroxy-2-naphthamide Hydrochloride (**42**). White powder (*m* = 40 mg, 61% yield); mp: 299–300 °C (dec.); <sup>1</sup>H NMR (DMSO-*d*<sub>6</sub>, 400 MHz): δ ppm 4.00 (s, 2H), 7.37 (m, 2H), 7.51 (m, 3H), 7.76 (d, 1H, *J* = 8.3 Hz), 7.80 (d, 2H, *J* = 8.4 Hz), 7.94 (d, 1H, *J* = 8.3 Hz), 8.35 (bs, 3H), 8.53 (s, 1H), 10.70 (s, 1H), 11.39 (bs, 1H); <sup>13</sup>C NMR (DMSO-*d*<sub>6</sub>, 100 MHz): δ ppm 41.8, 110.6, 120.4, 121.8, 123.7, 125.8, 126.9, 128.1, 128.7, 129.4, 129.6, 130.6, 135.8, 138.7, 153.6, 165.6; HPLC, RT = 1.26 min; HRMS calcd for C<sub>18</sub>H<sub>17</sub>N<sub>2</sub>O<sub>2</sub> 293.1285, found 293.1286.

*N*-(4-(Aminomethyl)phenyl)-2-naphthamide Hydrochloride (**43**). White powder (*m* = 26 mg, 61% yield); mp: 285–286 °C (dec.); <sup>1</sup>H NMR (DMSO-*d*<sub>6</sub>, 500 MHz): δ ppm 4.00 (q, 2H, *J* = 6.0 Hz), 7.50 (d, 2H, *J* = 8.5 Hz), 7.64 (m, 2H), 7.88 (d, 2H, *J* = 8.5 Hz), 8.01 (dd, 1H, *J* = 7.6, 1.4 Hz), 8.05 (m, 2H), 8.10 (dd, 1H, *J* = 7.3, 1.3 Hz), 8.47 (bs, 3H), 8.64 (s, 1H), 10.63 (s, 1H); <sup>13</sup>C NMR (DMSO-*d*<sub>6</sub>, 125 MHz): δ ppm 41.9, 120.3, 124.5, 126.9, 127.7, 128.0, 128.1, 128.2, 129.0, 129.2, 129.5, 132.0, 132.1, 134.3, 139.4, 165.7; HPLC, RT = 1.21 min; HRMS calcd for C<sub>18</sub>H<sub>17</sub>N<sub>2</sub>O<sub>2</sub> 277.1335, found 277.1326.

*N*-(4-(Aminomethyl)phenyl)-1H-indole-2-carboxamide (**44**). White solid (*m* = 40 mg, 76% yield); mp: 291–292 °C (dec.); <sup>1</sup>H NMR (DMSO-*d*<sub>6</sub>, 300 MHz): δ ppm 3.98 (q, 2H, *J* = 5.7 Hz), 7.07 (t, 1H, *J* = 7.8 Hz), 7.22 (t, 1H, *J* = 7.8 Hz), 7.47 (m, 4H), 7.67 (d, 1H, *J* = 8.0 Hz), 7.87 (d, 2H, *J* = 8.6 Hz), 8.40 (bs, 3H), 10.47 (s, 1H), 11.88 (s, 1H); <sup>13</sup>C NMR (DMSO-*d*<sub>6</sub>, 100 MHz): δ ppm 41.9, 104.4, 112.4, 119.9, 120.0, 121.8, 123.9, 127.0, 128.9, 129.5, 131.4, 136.8, 139.2, 159.7; HPLC, RT = 1.82 min; HRMS calcd for C<sub>16</sub>H<sub>16</sub>N<sub>3</sub>O 266.1288, found 266.1284.

*N*-(4-(Aminomethyl)phenyl)-4-oxo-1,4-dihydroquinoline-3-carboxamide (**45**). White solid (*m* = 65 mg, 99% yield); mp: 287–289 °C (dec.); <sup>1</sup>H NMR (DMSO-*d*<sub>6</sub>, 400 MHz): δ ppm 3.96 (q, 2H, *J* = 5.5 Hz), 7.50 (d, 2H, *J* = 8.4 Hz), 7.53 (td, 1H, *J* = 7.9, 1.3 Hz), 7.76 (d, 2H, *J* = 8.4 Hz), 7.79–7.86 (m, 2H), 8.31 (d, 1H, *J* = 7.9 Hz), 8.53 (bs, 3H), 8.82 (d, 1H, *J* = 6.7 Hz), 12.56 (s, 1H), 13.62 (d, 1H, *J* = 6.4 Hz); <sup>13</sup>C NMR (DMSO-*d*<sub>6</sub>, 100 MHz): δ ppm 41.8, 110.3, 119.2, 119.5, 125.3, 125.4, 125.9, 128.9, 129.9, 133.0, 138.9, 139.1, 143.9, 163.0, 176.3; HPLC, RT = 1.04 min; HRMS calcd for C<sub>17</sub>H<sub>16</sub>N<sub>3</sub>O<sub>2</sub> 294.1237, found 294.1247.

*N*-(4-(Aminomethyl)phenyl)-3-hydroxypyridine-2-carboxamide Hydrochloride (**46**). Beige solid (*m* = 28 mg, 44% yield); mp: 251–252 °C; <sup>1</sup>H NMR (DMSO-*d*<sub>6</sub>, 300 MHz): δ ppm 4.00 (q, 2H, *J* = 5.4 Hz), 4.78 (bs, 3H), 7.50 (m, 3H), 7.61 (dd, 1H, *J* = 8.5, 4.3 Hz), 7.87 (d, 2H, *J* = 8.6 Hz), 8.27 (dd, 1H, *J* = 4.3, 1.1 Hz), 8.35 (bs, 2H), 10.99 (s, 1H); <sup>13</sup>C NMR (DMSO-*d*<sub>6</sub>, 75 MHz): δ ppm 41.8, 121.3, 126.5, 129.4, 129.6, 130.2, 131.2, 137.3, 139.8, 157.6, 167.3; HPLC, RT = 0.95 min; HRMS calcd for C<sub>13</sub>H<sub>14</sub>N<sub>3</sub>O<sub>2</sub> 244.1081, found 244.1102.

*N*-(4-(Aminomethyl)phenyl)-6-methoxy-1-hydroxy-2-naphthamide Hydrochloride (**47**). Beige solid (*m* = 65 mg, 91% yield); mp: 256–257 °C (dec.); <sup>1</sup>H NMR (DMSO-*d*<sub>6</sub>, 300 MHz): δ ppm 3.91 (s, 3H), 4.02 (s, 2H), 7.19 (dd, 1H, *J* = 9.2, 2.5 Hz), 7.35 (m, 2H), 7.51 (d, 2H, *J* = 8.6 Hz), 7.77 (d, 2H, *J* = 8.6 Hz), 8.14 (d, 1H, *J* = 9.2 Hz), 8.20 (d, 1H, *J* = 9.2 Hz), 8.36 (bs, 3H), 10.55 (bs, 1H), 14.00 (s, 1H); <sup>13</sup>C NMR (DMSO-*d*<sub>6</sub>, 75 MHz): δ ppm 41.8, 55.4, 105.7, 106.4, 117.0, 117.9, 119.4, 122.0, 123.9, 125.0, 129.4, 130.1, 137.9, 138.1, 159.9, 160.3, 169.7; HPLC, RT = 1.36 min; HRMS calcd for C<sub>19</sub>H<sub>19</sub>N<sub>2</sub>O<sub>3</sub> 323.1390, found 323.1397.

*N*-(4-(Aminomethyl)phenyl)-7-methoxy-1-hydroxy-2-naphthamide Hydrochloride (**48**). White solid (*m* = 55 mg, 77% yield); mp: 250–251 °C; <sup>1</sup>H NMR (DMSO-*d*<sub>6</sub>, 400 MHz): δ ppm 3.91 (s, 3H), 4.02 (q, 2H, *J* = 5.0 Hz), 7.32 (dd, 1H, *J* = 8.9, 2.6 Hz), 7.42 (d, 1H, *J* = 8.8 Hz), 7.51 (d, 2H, *J* = 8.6 Hz), 7.60 (d, 1H, *J* = 2.6 Hz), 7.79 (d, 2H, *J* = 8.6 Hz), 7.85 (d, 1H, *J* = 8.9 Hz), 8.02 (d, 1H, *J* = 8.9 Hz), 8.36 (bs, 3H), 10.59 (s, 1H), 13.86 (s, 1H); <sup>13</sup>C NMR (DMSO-*d*<sub>6</sub>, 100 MHz): δ ppm 41.8, 55.2, 101.5, 107.9, 117.7, 120.6, 121.2, 122.1, 125.6, 129.2, 129.4, 130.1, 131.3, 137.8, 157.4, 158.8, 169.7; HPLC, RT = 1.37 min; HRMS calcd for C<sub>19</sub>H<sub>19</sub>N<sub>2</sub>O<sub>3</sub> 323.1390, found 323.1403.

*N*-(4-(Aminomethyl)phenyl)-7-methyl-1-hydroxy-2-naphthamide Hydrochloride (**49**). White solid (*m* = 53 mg, 77% yield); mp: 276–278 °C (dec.); <sup>1</sup>H NMR (DMSO-*d*<sub>6</sub>, 500 MHz): δ ppm 3.34 (s, 3H), 4.01 (s, 2H), 7.40 (d, 1H, *J* = 8.7 Hz), 7.51 (m, 3H), 7.80 (m, 3H), 8.08 (s, 1H), 8.12 (d, 1H, *J* = 8.7 Hz), 8.44 (bs, 3H), 10.62 (s, 1H), 13.94 (s, 1H); <sup>13</sup>C NMR (DMSO-*d*<sub>6</sub>, 125 MHz): δ ppm 21.4, 41.8, 107.5, 117.6, 122.0, 122.1, 122.2, 124.7, 127.4, 129.4, 130.2, 131.2, 134.2, 135.4, 137.8, 159.6, 169.7; HPLC, RT = 1.43 min; HRMS calcd for C<sub>19</sub>H<sub>19</sub>N<sub>2</sub>O<sub>2</sub> 307.1441, found 307.1452.

*N*-(4-(Aminomethyl)phenyl)-7-chloro-1-hydroxy-2-naphthamide Hydrochloride (**50**). White solid (*m* = 55 mg, 76%); mp: 277–278 °C; <sup>1</sup>H NMR (DMSO-*d*<sub>6</sub>, 500 MHz): δ ppm 4.02 (q, 2H, *J* = 5.6 Hz), 7.53 (m, 3H), 7.70 (dd, 1H, *J* = 8.8, 2.2 Hz), 7.79 (d, 2H, *J* = 8.6 Hz), 7.99 (d, 1H, *J* = 8.8 Hz), 8.24 (m, 2H), 8.39 (bs, 3H), 10.73 (s, 1H); <sup>13</sup>C NMR (DMSO-*d*<sub>6</sub>, 100 MHz): δ ppm 108.7, 117.8, 121.8, 122.2, 123.8, 125.4, 129.5, 129.6, 129.9, 130.4, 130.8, 134.4, 137.7, 158.8, 169.3; HPLC, RT = 1.49 min; HRMS calcd for C<sub>18</sub>H<sub>16</sub>N<sub>2</sub>O<sub>2</sub>Cl 327.0895, found 327.0890.

*N*-(4-(Aminomethyl)phenyl)-6,7-dimethoxy-1-hydroxy-2-naphthamide Hydrochloride (**51**). White solid (*m* = 62 mg, 80%); mp: 289–291 °C (dec.); <sup>1</sup>H NMR (DMSO-*d*<sub>6</sub>, 400 MHz): δ ppm 3.90 (s, 3H), 3.92 (s, 3H), 4.01 (q, 2H, *J* = 6.0 Hz), 7.31 (d, 1H, *J* = 8.8 Hz), 7.33 (s, 1H), 7.51 (d, 2H, *J* = 8.6 Hz), 7.55 (s, 1H), 7.79 (d, 2H, *J* = 8.6 Hz), 8.03 (d, 1H, *J* = 8.8 Hz), 8.45 (bs, 3H), 10.53 (s, 1H), 13.85 (s, 1H); <sup>13</sup>C NMR (DMSO-*d*<sub>6</sub>, 100 MHz): δ ppm 55.4, 55.6, 66.3, 101.8, 106.1, 106.7, 116.6, 119.2, 121.4, 121.9, 129.4, 130.0, 132.5, 137.9, 149.0, 151.6, 158.8, 169.8; HPLC, RT = 2.28 min; HRMS calcd for C<sub>20</sub>H<sub>21</sub>N<sub>2</sub>O<sub>4</sub> 353.1496, found 353.1496.

1-Hydroxy-*N*-piperidin-4-yl-2-naphthamide (**53**). White solid (*m* = 43 mg, 70% yield); mp: 279–280 °C; <sup>1</sup>H NMR (DMSO-*d*<sub>6</sub>, 400 MHz): δ ppm 1.89–2.02 (m, 4H), 3.02 (m, 2H), 3.33 (d, 2H, *J* = 12.8 Hz), 4.19 (m, 1H), 7.37 (d, 1H, *J* = 8.8 Hz), 7.55 (td, 1H, *J* = 8.1, 1.1 Hz), 7.63 (td, 1H, *J* = 8.1, 1.2 Hz), 7.87 (d, 1H, *J* = 8.1 Hz), 8.03 (d, 1H, *J* = 8.8 Hz), 8.25 (d, 1H, *J* = 8.1 Hz), 8.98 (d, 1H, *J* = 8.1 Hz), 9.08 (bs, 2H), 14.50 (s, 1H); <sup>13</sup>C NMR (DMSO-*d*<sub>6</sub>, 100 MHz): δ ppm 27.9, 44.5, 66.3, 106.9, 117.4, 122.9, 123.0, 124.6, 125.7, 127.4, 128.9, 135.8, 159.7, 170.1; HPLC, RT = 1.28 min; HRMS calcd for C<sub>16</sub>H<sub>19</sub>N<sub>2</sub>O<sub>2</sub> 271.1441, found 271.1439.

**Enzymes and Chemicals.** KLK6 was purchased from R&D Systems as pro-KLK6. Activation of KLK6 is performed in 50 mM Tris, 0.05% (w/v) Brij-35, pH 8.0. The activation reaction is initiated by lysyl-endopeptidase at 2.5 mU/mL (Wako Bioproducts). The activation reaction is stopped by diluting KLK6 to 0.5 μg/mL in assay buffer (50 mM Tris, 1 M citrate, 0.05% (w/v) Brij-35, pH 7.4) to obtain an active KLK6 stock. KLK1 was purchased from R&D Systems as pro-KLK1. Activation of KLK1 is performed in 50 mM Tris–HCl, 10 mM CaCl<sub>2</sub>, 150 mM NaCl, 0.05% Brij-35, pH 7.5. The activation reaction is initiated by bacterial thermolysin at 0.4 μg/mL (Sigma-Aldrich) and stopped by the addition of 100 mM ethyl-

enediaminetetraacetic acid (EDTA) (Sigma-Aldrich) to obtain an active KLK1 stock at the same concentration of 100 μg/mL. Plasmin (Sigma-Aldrich) and caspase-2, caspase-3, and caspase-6 (Enzo Life Sciences) were purchased in mature and active forms. All enzyme stocks were stored at –20 °C. KLK4, KLK5, KLK7, KLK8, KLK11, KLK13, thrombin, cathepsin L, matriptase, trypsin, trypsin-3, and tPA were purchased from R&D Systems as pro-enzymes (KLK4, KLK7, KLK8, KLK11, KLK13) or as mature and active forms (KLK5, thrombin, cathepsin L, matriptase, trypsin-3, tPA). Activation of KLK4, KLK7, KLK8, KLK11, and KLK13 is performed in optimized buffers. The activation reactions for KLK4, KLK7, and KLK11 are initiated bacterial thermolysin at 0.4 μg/mL (Sigma-Aldrich) and stopped by the addition of 100 mM EDTA (Sigma-Aldrich) to obtain active stocks. All enzyme stocks were stored at –20 °C. H-PFR-AMC (KLK1), Boc-VPR-AMC (KLK4, KLK5, KLK8, KLK13, KLK14, Thrombin), Boc-QAR-AMC (KLK6, KLK11, matriptase, trypsin, trypsin-3, plasmin), Ac-VDVAD-AMC (caspase-2), Ac-DEVD-AMC (caspase-3), Ac-VEID-AMC (caspase-6), Z-LR-AMC (cathepsin L), and Z-GGR-AMC (tPA) substrates were purchased from Bachem. MeO-Suc-RPY-AMC (KLK7) substrate was purchased from AAT Bioquest.

**Kinetics Assays.** Compounds were screened on KLK6, KLK1, and plasmin using a BMG Fluostar microplate reader (black 96-well microplates). The proteases are preincubated for 15 min with each compound (10 and 50 μM) or with DMSO (<2%, negative control) in a total volume of 100 μL of 50 mM Tris buffer, 1 M citrate, 0.05% Brij-35, pH 7, 37 °C. The reaction is triggered by adding the Boc-QAR-AMC (KLK6, plasmin) or H-PFR-AMC (KLK1) fluorogenic substrate (100 μM) and followed for 30 min at 37 °C. The release of the AMC fluorescent group is detected using the following wavelengths: λ<sub>ex</sub> = 360 nm for the excitation and λ<sub>em</sub> = 460 nm for the measurement of the emission. The percent inhibition is calculated from eq 1, where V<sub>0</sub> is the initial rate of the DMSO control and V<sub>i</sub> is the initial rate in the presence of the inhibitor.

$$\% \text{ inhibition} = (1 - (V_i/V_0)) \times 100 \quad (1)$$

The selected compounds are those for which the inhibition is greater than 50% at a concentration of 10 μM; then, IC<sub>50</sub> is determined. The inhibitory effect of the compound (%) as a function of its concentration generally follows eq 2a,b, which results in a hyperbole or a sigmoid. The equation is entered in the Kaleidagraph 4.5 software for curve fitting  $f([I]) = \% \text{ inhibition}$ , where [I] is the inhibitor concentration. The concentration ranges of inhibitor were adjusted to inhibitory potency as detected in preliminary screening tests; [I] was from 0.1 to 100 μM.

The inhibitory activity of compounds was expressed as IC<sub>50</sub> (inhibitor concentrations giving 50% inhibition). The values of IC<sub>50</sub> were calculated by fitting the experimental data to eq 2a,b

$$\% \text{ inhibition} = 100 \times (1 - V_i/V_0) = 100[I]_0 / (IC_{50} + [I]_0) \quad (2a)$$

$$\% \text{ inhibition} = 100[I]_0^{n_H} / (IC_{50}^{n_H} + [I]_0^{n_H}) \quad (2b)$$

where *n*<sub>H</sub> is the Hill number.

Reversibility was analyzed by diluting the reaction mixtures (dilution factor of 100) after 15 and 60 min preincubation of the enzyme with inhibitor. Aliquots of reaction mixtures (2.5 μL) were added to 97.5 μL of buffer containing the fluorogenic substrate (experimental conditions identical to the routine protocol used for a given enzyme). The mechanism of inhibition was determined by varying substrate and inhibitor concentrations, type of inhibition, and inhibition parameter (*K<sub>i</sub>*), which are determined by Dixon's plots.

**Selectivity Profiling.** Hit compounds were screened on the selected group of CNS proteases using optimized concentrations and buffers (KLK4 9.6 nM; KLK5 0.85 nM; KLK7 19 nM; KLK8 0.88 nM; KLK11 67 nM; KLK13 0.2 nM; KLK14 0.6 nM; caspase-2 0.2 nM; caspase-3 0.1 nM; caspase-6 68.5 mU/μL; cathepsin L 0.12 nM; matriptase 0.69 nM; thrombin 25 pM; tPA 6.7 nM; trypsin 0.63 pM; trypsin-3 0.8 pM; plasmin 3 nM). The reaction is triggered by the appropriate substrate at the optimized concentration (H-PFR-AMC

100  $\mu\text{M}$ ; Boc-VPR-AMC 100  $\mu\text{M}$ ; Boc-QAR-AMC 100  $\mu\text{M}$ ; Meo-Suc-RPY-AMC 100  $\mu\text{M}$ ; Ac-VDVAD-AMC 25  $\mu\text{M}$ ; Ac-DEVAD-AMC 10  $\mu\text{M}$ ; Ac-VEID-AMC 100  $\mu\text{M}$ ; Z-LR-AMC 50  $\mu\text{M}$ ; Z-GGR-AMC 100  $\mu\text{M}$ ) and followed for 30 min at 37 °C. Percentages of inhibition at 10  $\mu\text{M}$  of each compound are determined as described in the previous paragraph. Results are given from three independent experiments with a standard error below 10%.

**Molecular Docking.** Molecular docking experiments were conducted to propose interaction models of the hit *para*-aminobenzyl derivatives 32 and 42 with KLK6. The protonation states of the ligands were calculated using MarvinSketch at pH = 7. The major microspecies described the primary amine function charged, while the rest of the molecules were neutral (protonated alcohol function). The three-dimensional (3D) conformations of both ligands were generated by MarvinSketch. The structure of the target was retrieved from the Protein Data Bank (PDB) and chose due to the presence of an orthosteric inhibitor similar in structure to the *para*-aminobenzyl derivatives to shape the binding pocket to these two compounds (PDB id: 4D8N<sup>53,45</sup>). The protonation state of the target was predicted with Propka.<sup>46</sup> The catalytic histidine was found charged and protonated on both nitrogens, while other residues and termini were found in their canonical state at pH 7. The ligands and target were prepared using Autodock Tools 4<sup>47</sup> before flexible molecular docking with Autodock Vina.<sup>48</sup> Q192 and S195 side chains were found in different orientations in other KLK6 structures. These two residues were set flexible in the molecular docking routine to increase the reliability of the results. Including this protein flexibility, the number of degrees of freedom (dof) was still in an acceptable range for Vina (10 dof, while Vina is designed to converge properly until 12 dof). The box was centered near the geometrical center of the S1 binding pocket (residue: HS7, D189 to S195, S214 to N217, C220), with a final size of 18 × 19 × 18 Å<sup>3</sup>, which largely included S1, S1', S2, and S2'. Twenty poses were asked with an exhaustiveness of 128. The poses were then rescored using Convex-PL,<sup>49</sup> and the best poses according to this new scoring function of both compounds into KLK6 were further analyzed. The coordinate files of both poses are available in the online version.

**Neuronal Cytotoxicity of Hit Compounds.** All animals were ethically maintained and used in compliance with the European Policy on Ethics. Cortices and striatum were microdissected from E14 embryos of Swiss mice (Janvier, Labs Le Genest Saint Isle, France) in Dulbecco's phosphate-buffered saline (DPBS) supplemented with 0.1% (w/w) glucose (Thermo Fisher Scientific; 15023-021). Dissected structures were digested with trypsin/EDTA (Thermo Fisher Scientific; R001100) for 15 min at room temperature. After trypsin inactivation with 10% (v/v) fetal bovine serum (FBS) (10500056; Thermo Fisher Scientific), structures were mechanically dissociated with a pipette in Neurobasal media (Thermo Fisher Scientific; 2110349) supplemented with DNase I (Thermo Fisher Scientific; EN0525), B27 (Thermo Fisher Scientific; 17504-044), L-glutamine (Thermo Fisher Scientific; 25030-024), and penicillin/streptomycin (Thermo Fisher Scientific, 1540-122). Cortical and striatal cells were then seeded at the density of 100 000 cells/well in sterile transparent 96-well plates previously coated. The cells are cultured for 7 days at 37 °C in a 5% CO<sub>2</sub> atmosphere. The cells were treated for 24 h with inhibitors at different concentrations (10, 25, 50, or 100  $\mu\text{M}$ ), with the vehicle DMSO 1% (negative control, vehicle), or with rotenone 50  $\mu\text{M}$  (positive control). The treatment of primary cultures of neurons by rotenone is a standard compound used to induce neuronal death. The medium is then replaced with 50  $\mu\text{L}$  of XTT (0.3 mg/mL) for 3 h to carry out the cell viability test (Merck; 11465015001). XTT is a derivative of tetrazolium salt whose reduction by mitochondrial dehydrogenase viable cells shows a yellow-orange coloring. The activity of the mitochondria is determined by measuring the absorbance at 485 nm. The percentage of cell survival is calculated by the ratio of the absorbance in the presence of the inhibitor to the negative control condition (DMSO 1%). Statistical analyses of differences between treatments were assessed by a Kruskal–Wallis test using GraphPad Prism 7.03. For all analysis, \**p*-value <0.05; \*\**p*-value <0.01; \*\*\**p*-value <0.001.

**Evaluation of the Effect of Compounds on Oligodendrocyte Differentiation. B104 Cell Culture.** B104 cells were cultured in flasks (TPP) containing Dulbecco's modified Eagle's medium (DMEM) (Gibco) supplemented with 1% penicillin–streptomycin (Gibco), 1% nonessential amino acids (NEAA) solution (Gibco), and 10% fetal bovine serum (FBS; Gibco) and passaged every week using trypsin 0.25% (Gibco; 25200056). This medium was changed after 4 days for N1 medium w/o biotin. This B104-conditioned medium containing growth factors was collected after 3 days and used to prepare N1B104 medium.

**CG4 Cell Line Culture.** CG4 cells were cultured in culture flasks (TPP) coated with 0.01% poly-L-ornithine (Sigma) with filtered N1B104 medium to ensure proliferation. The cells were passaged with trypsin 0.05% (Gibco) when reaching 60–70% confluence.<sup>52</sup> The CG4 line used in this study expressed the fluorescent reporters GFP at all developmental stages of the oligodendroglial cell lineage and mCherry only in differentiated and mature oligodendrocytes.

For differentiation assay, CG4 cells were seeded in N1B104 medium in 96-well plates (Nunc) at the density of 6500 cell/cm<sup>2</sup> for a few hours. The cells were then switched in a differentiation medium (DMEM/F12 1:1 (Gibco) supplemented with 2% B27 (Gibco); 1% laminin (Sigma) and 1% N1 biotin) with or without the compounds. The 9-*cis*-retinoic acid at 1  $\mu\text{M}$  (Sigma) was used as a positive control. The cells were differentiated for 5 days before image acquisition and quantification on an Arrayscan XTI System (Thermo Scientific).

**Oligodendrocyte Precursor Cell (OPCs) Primary Cell Cultures.** Primary OPCs cultured were derived from Wistar rats' cerebral cortices at P1, as previously described.<sup>50</sup> Briefly, the cerebral cortices were dissected and the meninges were removed in DME, 1% penicillin–streptomycin, and 1% MEM NEAA. Tissues were dissociated enzymatically using trypsin–EDTA solution for 10 min at 37 °C. The cell suspension was filtered with 70  $\mu\text{m}$  nylon cell strainer, centrifuged at 1000 rpm for 10 min, and resuspended in an appropriate volume of DMEM/10% FBS for seeding (10 mL per flask/two brains in each) in culture flasks coated with 0.01% poly-L-ornithine and incubated at 5% CO<sub>2</sub> and 37 °C for approximately 2 weeks. The medium was changed on day 7. After 14 days, the cells were shaken for 2 h at 250 rpm to remove microglia.<sup>51</sup> An additional shaking is performed overnight at 250 rpm to detach and collect OPCs. Collected OPCs were plated on polyornithine coated 24-well plates, at a density of 25 000 cells/well. OPCs were kept in proliferation medium containing DMEM/F12 (1:1) and supplemented with 2% B27 (all purchased from Gibco), FGF, and PDGF (10 ng/mL each) to allow adhesion. The medium is then changed for a differentiation medium with or without the compounds. As for the CG4 cultures, 9-*cis*-retinoic acid at 1  $\mu\text{M}$  was used as a positive control. The cells were kept in differentiation medium for 5 days, before image acquisition and quantification on an Arrayscan XTI System (Thermo Scientific).

**Immunostaining.** Cells were fixed with 2% paraformaldehyde (electron microscopy) for 5 min at room temperature, washed with phosphate-buffered saline (PBS) 1×, and stored at 4 °C prior to staining. They were incubated for 1 h at RT in 4% bovine serum albumin (BSA) (Sigma), 1× PBS, 0.1% Triton X-100, and primary antibodies. They were next rinsed three times with PBS 1× and incubated for 45 min at RT in 4% BSA in 1× PBS, 1  $\mu\text{g}/\text{mL}$  Hoechst dye (Sigma, B2261), and secondary antibodies. After incubation, plates were washed three times with PBS 1×. Image acquisitions and quantification were performed as described above.

The line used is a rat oligodendrocyte precursor (CG4) CG4 cell line, stably transduced with the GFP reporter gene under the control of the CMV promoter and mCherry under the control of a differentiated oligodendrocyte-specific promoter. The mCherry marker is only expressed at the differentiated oligodendrocyte stage and thus makes it possible to test compounds capable of inducing differentiation of OPCs. The cells are cultured in the proliferation medium described by Louis et al.<sup>52</sup> at the time of their enumeration, then in a medium of differentiation (DMEM/F12, B27, N1, biotin, laminin). The cells are treated with different inhibitor concentrations for 72 h in 96-well plates and then screened using an automated

inverted microscope. The experimental controls used are a basal control containing only the differentiation medium and a positive control, 9-*cis*-retinoic acid, known for its effect in inducing differentiation of OPCs.<sup>53</sup> To evaluate the effects of the compounds on OPC differentiation, we quantified the number of mCherry+ and GFP+ cells under each experimental condition relative to the basal control. An effect in favor of differentiation is reflected in a significant increase in the number of mCherry+ cells, in contrast to an effect to the detriment of differentiation. The results are analyzed using the Mann–Whitney statistical test.

**Anti-inflammatory Potential.** The impact of compounds on microglial activation and proinflammatory cytokines was assessed in purified primary microglial cultures isolated from newborn rat brain, as previously described.<sup>36</sup> All animals used were handled in accordance with European standards for ethics and animal welfare. The newborn Wistar rats (Janvier Labs, Le Genest Saint Isle, France) at stage P1 are sacrificed by decapitation. After removal of the meninges, the cortical structures are removed in DMEM containing 1% penicillin/streptomycin mix (Thermo Fisher, 15070063) and 1% nonessential amino acids (MEM NEAA, Thermo Fisher, 11140050). Tissues are enzymatically dissociated by the addition of trypsin–EDTA (Gibco, 25200056) for 10 min at 37 °C. The cell suspension is then passed through a nylon filter 70 μm in diameter, centrifuged at 1000 rpm for 10 min, and then resuspended in 10 mL of DMEM supplemented with 10% fetal calf serum (FCS) (Thermo Fisher Scientific, 10500056) in a flask previously coated with 0.01% poly-L-ornithine (Sigma-Aldrich, P4957). The cells are cultured for 2 weeks at 37 °C in a humid atmosphere (5% CO<sub>2</sub>) with a change of medium on the 7th day. At the end of this period, the cells are stirred for 2 h at 250 rpm to detach and recover the microglia. The cells are inoculated into sterile transparent 96-well FALCON plates at a density of 50 000 cells/well in DMEM/F12 medium supplemented with 1% N<sub>2</sub> mix and then cultured for 24 h at 37 °C in a humid atmosphere (5% CO<sub>2</sub>). The microglia is treated with lipopolysaccharide (LPS, 10 ng/mL, Sigma-Aldrich) to create an inflammatory environment to be activated. Concomitantly, the cells are treated with inhibitors at different concentrations defined according to the IC<sub>50</sub> values (0.5–10 μM), with 1% DMSO (negative control), or with 100 nM dexamethasone (positive anti-inflammatory control, Sigma-Aldrich, D4902) for 3 h at 37 °C in a humid atmosphere (5% CO<sub>2</sub>). At the end of this incubation, supernatants are recovered for assays of proinflammatory cytokines TNF-α and IL1-β by ELISA (Rat TNF-α ELISA MAXTM Deluxe Set # 438204, rat IL1-β ELISA kit ab100768).

## ■ ASSOCIATED CONTENT

### SI Supporting Information

The Supporting Information is available free of charge at <https://pubs.acs.org/doi/10.1021/acs.jmedchem.0c02175>.

Compounds' synthesis and characterization data; Dixon plot of compounds 37 and 47 toward KLK6 (Figure S1); structures of synthesized compounds (Table S1); and comparison of ADME and pharmacological parameters for hit compounds 32 and 42 (Table S2) (PDF)

Molecular formula strings of compounds described in this study (CSV)

Models of compound 32 on 4D8N KLK6 (PDB)

Models of compound 42 docked on 4D8N KLK6 (PDB)

## ■ AUTHOR INFORMATION

### Corresponding Authors

Brahim Nait Oumesmar – *Institut du Cerveau, Inserm U 1127, CNRS UMR 7725, Sorbonne Université, F-75013*

Paris, France; Email: [brahim.nait\\_oumesmar@sorbonne-universite.fr](mailto:brahim.nait_oumesmar@sorbonne-universite.fr)

Nicolas Masurier – *Institut des Biomolécules Max Mousseron, Université de Montpellier, CNRS, ENSCM, F-34093 Montpellier, France; Email: [nicolas.masurier@umontpellier.fr](mailto:nicolas.masurier@umontpellier.fr)*

Chahrazade El Amri – *Faculty of Sciences and Engineering, IBPS, UMR 8256 CNRS-UPMC, ERL INSERM U1164, Biological Adaptation and Ageing, Sorbonne Université, F-75252 Paris, France; [orcid.org/0000-0002-1028-5113](https://orcid.org/0000-0002-1028-5113); Email: [chahrazade.el\\_amri@sorbonne-universite.fr](mailto:chahrazade.el_amri@sorbonne-universite.fr)*

## Authors

Sabrina Ait Amiri – *Faculty of Sciences and Engineering, IBPS, UMR 8256 CNRS-UPMC, ERL INSERM U1164, Biological Adaptation and Ageing, Sorbonne Université, F-75252 Paris, France*

Cyrille Deboux – *Institut du Cerveau, Inserm U 1127, CNRS UMR 7725, Sorbonne Université, F-75013 Paris, France*

Feryel Soualmia – *Faculty of Sciences and Engineering, IBPS, UMR 8256 CNRS-UPMC, ERL INSERM U1164, Biological Adaptation and Ageing, Sorbonne Université, F-75252 Paris, France*

Nancy Chaaya – *Faculty of Sciences and Engineering, IBPS, UMR 8256 CNRS-UPMC, ERL INSERM U1164, Biological Adaptation and Ageing, Sorbonne Université, F-75252 Paris, France*

Maxime Louet – *Institut des Biomolécules Max Mousseron, Université de Montpellier, CNRS, ENSCM, F-34093 Montpellier, France*

Eric Duplus – *Faculty of Sciences and Engineering, IBPS, UMR 8256 CNRS-UPMC, ERL INSERM U1164, Biological Adaptation and Ageing, Sorbonne Université, F-75252 Paris, France*

Sandrine Betuing – *Faculty of Sciences and Engineering, IBPS, UMR 8246-CNRS/INSERM U1130, Neurosciences Paris Seine, Sorbonne Université, F-75252 Paris, France*

Complete contact information is available at: <https://pubs.acs.org/doi/10.1021/acs.jmedchem.0c02175>

## Author Contributions

The research was designed by C.E., N.M., and B.N.O. Chemical synthesis was performed by N.M. Enzymology assays were performed by S.A.A., N.C., and F.S.; biological assays were performed with neural cells, OPCs, and microglial cells by S.A.A. and C.D. Docking models were determined by M.L. E.D. and S.B. contributed to experiments on primary cultures of neural cells. Data analysis and manuscript preparation were done by C.E.A., N.M., and B.N.O. All of the authors have given approval the final version of the manuscript.

## Notes

The authors declare no competing financial interest.

## ■ ACKNOWLEDGMENTS

The authors are grateful to Sorbonne Université, Université de Montpellier, Institut National pour la Recherche Médicale (INSERM), Centre National de la Recherche Scientifique (CNRS), Fondation pour la recherche sur la sclérose en plaques (ARSEP Fondation), as well as the SATT Lutech for research funding. The authors thank Dr. David Akbar (ICM Cell Culture Facility, CELIS) for his advice and technical

assistance on fluorescence imaging and quantitative analysis. This study was supported by the Investissements d'Avenir ANR-10-IAIHU-06 (IHU-A-ICM) and ANR-11-INBS-0011 (NeurATRIS) (to B.N.O.). The authors thank the French Ministry of Research and Education for S.A.A. and F.S. Ph.D. fellowships.

## ABBREVIATIONS

ADMET, absorption diffusion metabolism, elimination, and toxicity; CNS, central nervous system; DMEM, Dulbecco's modified Eagle's medium; DMSO, dimethyl sulfoxide; EDCI, *N*-(3-dimethylaminopropyl)-*N'*-ethylcarbodiimide hydrochloride; IL1 $\beta$ , interleukin 1  $\beta$ ; KLK, tissue kallikreins; KLK1, kallikrein-related peptidase 1; KLK6, kallikrein-related peptidase 6; LPS, lipopolysaccharide; MBP, myelin basic protein; MS, multiple sclerosis; OPC, oligodendrocyte precursor cell; PAR, protease-activated receptors; TNF  $\beta$ , tumor necrosis factor

## REFERENCES

- (1) Lassmann, H. Multiple Sclerosis Pathology. *Cold Spring Harbor Perspect. Med.* **2018**, *8*, No. a028936.
- (2) Friese, M. A.; Schattling, B.; Fugger, L. Mechanisms of neurodegeneration and axonal dysfunction in multiple sclerosis. *Nat. Rev. Neurol.* **2014**, *10*, 225–238.
- (3) Kuhlmann, T.; Miron, V.; Cui, Q.; Wegner, C.; Antel, J.; Bruck, W. Differentiation block of oligodendroglial progenitor cells as a cause for remyelination failure in chronic multiple sclerosis. *Brain* **2008**, *131*, 1749–1758.
- (4) Bove, R. M.; Green, A. J. Remyelinating Pharmacotherapies in Multiple Sclerosis. *Neurotherapeutics* **2017**, *14*, 894–904.
- (5) Cole, K. L. H.; Early, J. J.; Lyons, D. A. Drug discovery for remyelination and treatment of MS. *Glia* **2017**, *65*, 1565–1589.
- (6) Franklin, R. J. M.; Ffrench-Constant, C. Regenerating CNS myelin - from mechanisms to experimental medicines. *Nat. Rev. Neurosci.* **2017**, *18*, 753–769.
- (7) Coetzee, T.; Thompson, A. J. Unified understanding of MS course is required for drug development. *Nat. Rev. Neurol.* **2018**, *14*, 191–192.
- (8) Cunniffe, N.; Coles, A. Promoting remyelination in multiple sclerosis. *J. Neurol.* **2021**, *268*, 30–44.
- (9) Murakami, K.; Jiang, Y. P.; Tanaka, T.; Bando, Y.; Mitrovic, B.; Yoshida, S. In vivo analysis of kallikrein-related peptidase 6 (KLK6) function in oligodendrocyte development and the expression of myelin proteins. *Neuroscience* **2013**, *236*, 1–11.
- (10) Bando, Y.; Ito, S.; Nagai, Y.; Terayama, R.; Kishibe, M.; Jiang, Y. P.; Mitrovic, B.; Takahashi, T.; Yoshida, S. Implications of protease M/neurosin in myelination during experimental demyelination and remyelination. *Neurosci. Lett.* **2006**, *405*, 175–180.
- (11) Scarisbrick, I. A.; Isackson, P. J.; Ciric, B.; Windebank, A. J.; Rodriguez, M. MSP, a trypsin-like serine protease, is abundantly expressed in the human nervous system. *J. Comp. Neurol.* **2001**, *431*, 347–361.
- (12) Bando, Y.; Hagiwara, Y.; Suzuki, Y.; Yoshida, K.; Aburakawa, Y.; Kimura, T.; Murakami, C.; Ono, M.; Tanaka, T.; Jiang, Y. P.; Mitrovic, B.; Bochimoto, H.; Yahara, O.; Yoshida, S. Kallikrein 6 secreted by oligodendrocytes regulates the progression of experimental autoimmune encephalomyelitis. *Glia* **2018**, *66*, 359–378.
- (13) Burda, J. E.; Radulovic, M.; Yoon, H.; Scarisbrick, I. A. Critical role for PAR1 in kallikrein 6-mediated oligodendroglial pathology. *Glia* **2013**, *61*, 1456–1470.
- (14) Yoon, H.; Radulovic, M.; Scarisbrick, I. A. Kallikrein-related peptidase 6 orchestrates astrocyte form and function through proteinase activated receptor-dependent mechanisms. *Biol. Chem.* **2018**, *399*, 1041–1052.
- (15) Yoon, H.; Radulovic, M.; Walters, G.; Paulsen, A. R.; Drucker, K.; Starski, P.; Wu, J.; Fairlie, D. P.; Scarisbrick, I. A. Protease activated receptor 2 controls myelin development, resiliency and repair. *Glia* **2017**, *65*, 2070–2086.
- (16) Radulovic, M.; Yoon, H.; Wu, J.; Mustafa, K.; Scarisbrick, I. A. Targeting the thrombin receptor modulates inflammation and astrogliosis to improve recovery after spinal cord injury. *Neurobiol. Dis.* **2016**, *93*, 226–242.
- (17) Panos, M.; Christophi, G. P.; Rodriguez, M.; Scarisbrick, I. A. Differential expression of multiple kallikreins in a viral model of multiple sclerosis points to unique roles in the innate and adaptive immune response. *Biol. Chem.* **2014**, *395*, 1063–1073.
- (18) Kroksveen, A. C.; Aasebo, E.; Vethe, H.; Van Pesch, V.; Franciotta, D.; Teunissen, C. E.; Ulvik, R. J.; Vedeler, C.; Myhr, K. M.; Barsnes, H.; Berven, F. S. Discovery and initial verification of differentially abundant proteins between multiple sclerosis patients and controls using iTRAQ and SID-SRM. *J. Proteomics* **2013**, *78*, 312–325.
- (19) Scarisbrick, I. A. The multiple sclerosis degradome: enzymatic cascades in development and progression of central nervous system inflammatory disease. *Curr. Top. Microbiol. Immunol.* **2008**, *318*, 133–175.
- (20) Blaber, S. I.; Ciric, B.; Christophi, G. P.; Bernett, M. J.; Blaber, M.; Rodriguez, M.; Scarisbrick, I. A. Targeting kallikrein 6 proteolysis attenuates CNS inflammatory disease. *FASEB J.* **2004**, *18*, 920–932.
- (21) Yoon, H.; Blaber, S. I.; Evans, D. M.; Trim, J.; Juliano, M. A.; Scarisbrick, I. A.; Blaber, M. Activation profiles of human kallikrein-related peptidases by proteases of the thrombostasis axis. *Protein Sci.* **2008**, *17*, 1998–2007.
- (22) Shaw, M. A.; Gao, Z.; McElhinney, K. E.; Thornton, S.; Flick, M. J.; Lane, A.; Degen, J. L.; Ryu, J. K.; Akassoglou, K.; Mullins, E. S. Plasminogen Deficiency Delays the Onset and Protects from Demyelination and Paralysis in Autoimmune Neuroinflammatory Disease. *J. Neurosci.* **2017**, *37*, 3776–3788.
- (23) Balashov, K.; Dhib-Jalbut, S.; Rybinnik, I. Fibrinolysis induced clinical improvement in a patient with multiple sclerosis exacerbation. *Mult. Scler. Relat. Disord.* **2020**, *43*, No. 102225.
- (24) Masurier, N.; Arama, D. P.; El Amri, C.; Lisowski, V. Inhibitors of kallikrein-related peptidases: An overview. *Med. Res. Rev.* **2018**, *38*, 655–683.
- (25) Prassas, I.; Eissa, A.; Poda, G.; Diamandis, E. P. Unleashing the therapeutic potential of human kallikrein-related serine proteases. *Nat. Rev. Drug Discovery* **2015**, *14*, 183–202.
- (26) Masurier, N.; Soualmia, F.; Sanchez, P.; Lefort, V.; Roué, M.; Maillard, L.; Subra, G.; Percot, A.; El Amri, C. Synthesis of Peptide–Adenine Conjugates as a New Tool for Monitoring Protease Activity. *Eur. J. Org. Chem.* **2019**, *2019*, 176–183.
- (27) Loessner, D.; Goettig, P.; Preis, S.; Felber, J.; Bronger, H.; Clements, J. A.; Dorn, J.; Magdolen, V. Kallikrein-related peptidases represent attractive therapeutic targets for ovarian cancer. *Expert Opin. Ther. Targets* **2018**, *22*, 745–763.
- (28) Goettig, P.; Magdolen, V.; Brandstetter, H. Natural and synthetic inhibitors of kallikrein-related peptidases (KLKs). *Biochimie* **2010**, *92*, 1546–1567.
- (29) Sananes, A.; Cohen, I.; Shahar, A.; Hockla, A.; De Vita, E.; Miller, A. K.; Radisky, E. S.; Papo, N. A potent, proteolysis-resistant inhibitor of kallikrein-related peptidase 6 (KLK6) for cancer therapy, developed by combinatorial engineering. *J. Biol. Chem.* **2018**, *293*, 12663–12680.
- (30) De Vita, E.; Schuler, P.; Lovell, S.; Lohbeck, J.; Kullmann, S.; Rabinovich, E.; Sananes, A.; Hessling, B.; Hamon, V.; Papo, N.; Hess, J.; Tate, E. W.; Gunkel, N.; Miller, A. K. Depsipeptides Featuring a Neutral P1 Are Potent Inhibitors of Kallikrein-Related Peptidase 6 with On-Target Cellular Activity. *J. Med. Chem.* **2018**, *61*, 8859–8874.
- (31) Soualmia, F.; Bosc, E.; Ait Amiri, S.; Stratmann, D.; Magdolen, V.; Darmoul, D.; Reboud-Ravaux, M.; El Amri, C. Insights into the activity control of the kallikrein-related peptidase 6: small-molecule modulators and allostery. *Biol. Chem.* **2018**, *399*, 1073–1078.
- (32) De Vita, E.; Smits, N.; van den Hurk, H.; Beck, E. M.; Hewitt, J.; Baillie, G.; Russell, E.; Pannifer, A.; Hamon, V.; Morrison, A.; McElroy, S. P.; Jones, P.; Ignatenko, N. A.; Gunkel, N.; Miller, A. K.

Synthesis and Structure-Activity Relationships of N-(4-Benzamidino)-Oxazolidinones: Potent and Selective Inhibitors of Kallikrein-Related Peptidase 6. *ChemMedChem* **2020**, *15*, 79–95.

(33) Liang, G.; Chen, X.; Aldous, S.; Pu, S. F.; Mehdi, S.; Powers, E.; Xia, T.; Wang, R. Human kallikrein 6 inhibitors with a paramidobenzylamine P1 group identified through virtual screening. *Bioorg. Med. Chem. Lett.* **2012**, *22*, 2450–2455.

(34) Skaper, S. D. Oligodendrocyte precursor cells as a therapeutic target for demyelinating diseases. *Prog. Brain Res.* **2019**, *245*, 119–144.

(35) Voet, S.; Prinz, M.; van Loo, G. Microglia in Central Nervous System Inflammation and Multiple Sclerosis Pathology. *Trends Mol. Med.* **2019**, *25*, 112–123.

(36) Tamashiro, T. T.; Dalgard, C. L.; Byrnes, K. R. Primary microglia isolation from mixed glial cell cultures of neonatal rat brain tissue. *J. Visualized Exp.* **2012**, *15*, No. e3814.

(37) Bowes, J.; Brown, A. J.; Hamon, J.; Jarolimek, W.; Sridhar, A.; Waldron, G.; Whitebread, S. Reducing safety-related drug attrition: the use of in vitro pharmacological profiling. *Nat. Rev. Drug Discovery* **2012**, *11*, 909–922.

(38) Strauss, K. I. Antiinflammatory and neuroprotective actions of COX2 inhibitors in the injured brain. *Brain, Behav., Immun.* **2008**, *22*, 285–298.

(39) Katayama, K.; Arai, Y.; Murata, K.; Saito, S.; Nagata, T.; Takashima, K.; Yoshida, A.; Masumura, M.; Koda, S.; Okada, H.; Muto, T. Discovery and structure-activity relationships of spiroindolines as novel inducers of oligodendrocyte progenitor cell differentiation. *Bioorg. Med. Chem.* **2020**, *28*, No. 115348.

(40) Zaldivar-Diez, J.; Li, L.; Garcia, A. M.; Zhao, W. N.; Medina-Menendez, C.; Haggarty, S. J.; Gil, C.; Morales, A. V.; Martinez, A. Benzothiazole-Based LRRK2 Inhibitors as Wnt Enhancers and Promoters of Oligodendrocytic Fate. *J. Med. Chem.* **2020**, *63*, 2638–2655.

(41) Su, W.; Matsumoto, S.; Banine, F.; Srivastava, T.; Dean, J.; Foster, S.; Pham, P.; Hammond, B.; Peters, A.; Girish, K. S.; Rangappa, K. S.; Basappa, S.; Jose, J.; Hennebold, J. D.; Murphy, M. J.; Bennett-Toomey, J.; Back, S. A.; Sherman, L. S. A modified flavonoid accelerates oligodendrocyte maturation and functional remyelination. *Glia* **2020**, *68*, 263–279.

(42) Darensbourg, D. J.; Chung, W. C.; Arp, C. J.; Tsai, F. T.; Kyran, S. J. Copolymerization and Cycloaddition Products Derived from Coupling Reactions of 1,2-Epoxy-4-cyclohexene and Carbon Dioxide. Postpolymerization Functionalization via Thiol–Ene Click Reactions. *Macromolecules* **2014**, *47*, 7347–7353.

(43) Tanaka, K. I.; Yoshifuji, S.; Nitta, Y. A New Method for the Synthesis of Amides from Amines: Ruthenium Tetroxide Oxidation of N-Protected Alkylamines. *Chem. Pharm. Bull.* **1988**, *36*, 3125–3129.

(44) Gallo-Rodriguez, C.; Ji, X. D.; Melman, N.; Siegman, B. D.; Sanders, L. H.; Orlina, J.; Fischer, B.; Pu, Q.; Olah, M. E.; van Galen, P. J.; Stiles, G. L.; Jacobson, K. A. Structure-activity relationships of N6-benzyladenosine-5'-uronamides as A3-selective adenosine agonists. *J. Med. Chem.* **1994**, *37*, 636–646.

(45) Liang, G.; Chen, X.; Aldous, S.; Pu, S. F.; Mehdi, S.; Powers, E.; Giovanni, A.; Kongsamut, S.; Xia, T.; Zhang, Y.; Wang, R.; Gao, Z.; Merriman, G.; McLean, L. R.; Morize, I. Virtual Screening and X-ray Crystallography for Human Kallikrein 6 Inhibitors with an Amidinothiophene P1 Group. *ACS Med. Chem. Lett.* **2012**, *3*, 159–164.

(46) Olsson, M.; Søndergaard, C. R.; Rostkowski, M.; Jensen, J. H. PROPKA3: Consistent Treatment of Internal and Surface Residues in Empirical pKa Predictions. *J. Chem. Theory Comput.* **2011**, *7*, 525–537.

(47) Morris, G. M.; Huey, R.; Lindstrom, W.; Sanner, M. F.; Belew, R. K.; Goodsell, D. S.; Olson, A. J. AutoDock4 and AutoDockTools4: Automated docking with selective receptor flexibility. *J. Comput. Chem.* **2009**, *30*, 2785–2791.

(48) Trott, O.; Olson, A. J. AutoDock Vina: improving the speed and accuracy of docking with a new scoring function, efficient

optimization and multithreading. *J. Comput. Chem.* **2010**, *31*, 455–461.

(49) Kadukova, M.; Grudin, S. Convex-PL: a novel knowledge-based potential for protein-ligand interactions deduced from structural databases using convex optimization. *J. Comput.-Aided Mol. Des.* **2017**, *31*, 943–958.

(50) Wegener, A.; Deboux, C.; Bachelin, C.; Frah, M.; Kerninon, C.; Seilhean, D.; Weider, M.; Wegner, M.; Nait-Oumesmar, B. Gain of Olig2 function in oligodendrocyte progenitors promotes remyelination. *Brain* **2015**, *138*, 120–135.

(51) de Vellis, J.; Cole, R. Preparation of mixed glial cultures from postnatal rat brain. *Methods Mol. Biol.* **2012**, *814*, 49–59.

(52) Louis, J. C.; Magal, E.; Muir, D.; Manthorpe, M.; Varon, S. CG-4, a new bipotential glial cell line from rat brain, is capable of differentiating in vitro into either mature oligodendrocytes or type-2 astrocytes. *J. Neurosci. Res.* **1992**, *31*, 193–204.

(53) Huang, J. K.; Jarjour, A. A.; Nait Oumesmar, B.; Kerninon, C.; Williams, A.; Krezel, W.; Kagechika, H.; Bauer, J.; Zhao, C.; Baron-Van Evercooren, A.; Chambon, P.; Ffrench-Constant, C.; Franklin, R. J. M. Retinoid X receptor gamma signaling accelerates CNS remyelination. *Nat. Neurosci.* **2011**, *14*, 45–53.